

Multiple quadrupolar or nematic phases driven by the Heisenberg interactions in a spin-1 dimer system forming a bilayer

Katsuhiko Tanaka and Chisa Hotta

Department of Basic Science, University of Tokyo, Meguro, Tokyo 153-8902, Japan

(Received 29 December 2019; revised manuscript received 24 February 2020; accepted 26 February 2020; published 18 March 2020)

We explore several classes of quadrupolar ordering in a system of antiferromagnetically coupled quantum spin-1 dimers, which are stacked in the triangular lattice geometry forming a bilayer. Low-energy properties of this model are described by an $S = 1$ hard-core bosonic degrees of freedom defined on each dimer bond, where the singlet and triplet states of the dimerized spins are interpreted as the vacuum and the occupancy of boson, respectively. The number of bosons per dimer and the magnetic and density fluctuations of bosons are controlled by the interdimer Heisenberg interactions. In a solid phase where each dimer hosts one boson and the interdimer interaction is weak, a conventional spin nematic phase is realized by the pair fluctuation of bosons. Larger interdimer interaction favors Bose-Einstein condensates (BEC) carrying quadrupolar moments. Among them, we find one exotic phase where the quadrupoles develop a spatially modulated structure on the top of a uniform BEC, interpreted in the original dimerized spin-1 model as coexistent p -type nematic and 120° magnetic correlations. This may explain an intriguing nonmagnetic phase found in $\text{Ba}_3\text{ZnRu}_2\text{O}_9$.

DOI: [10.1103/PhysRevB.101.094422](https://doi.org/10.1103/PhysRevB.101.094422)

I. INTRODUCTION

Nematics, regarded as a sort of liquid crystal in a more general context, now forms a wide range of phases of matter in crystalline solids. The “electronic nematic state” was first proposed in a doped Mott insulator as a consequence of the melting of stripes, aiming to understand the origin of high- T_c phase in cuprates [1]. A more recent example is the nematicity of electronic wave functions induced by the orbital ordering in iron-based superconductors, possibly dominating the stability of the superconductivity [2–4]. When defined on a crystal lattice, the nematics of charges and orbitals, and also of spins, are all described by the quadrupolar order parameter representing the symmetry of their wave function.

In insulating quantum magnets [5,6], nematic phases appear when the spin moments break their rotational symmetry and form a wave function in the shape of rodlike or disklike director which collectively align in space. The search of spin nematics has been a challenge since proposals relevant to experiments are provided only in limited numbers of systems; in a layered solid ^3He [7], in an artificially designed optical lattice [8,9], and in a quantum spin- $\frac{1}{2}$ magnet near the saturation field [10–12].

There had been some reasons that the quantum spin systems cannot easily become a good platform of spin nematics. In materials, the electrons carry spin $\frac{1}{2}$, which is a dipole by itself, and to form a quadrupole which is a rank-2 tensor, we need at least spin 1 with three different S^z levels [see Eq. (8)]. There are two ways to construct spin 1 from spin $\frac{1}{2}$. One is to use the Hund’s coupling between spin $\frac{1}{2}$ in different orbitals on the same site, which will generate *site* nematics. The other is to efficiently compose spin 1 from two spin $\frac{1}{2}$ ’s

on neighboring sites by the interaction, in which case the *bond* nematic is formed. In the former case, a quantum spin-1 bilinear-biquadratic (BLBQ) model is known to host a spin nematic phase for a large biquadratic interaction $(\mathbf{S}_i \cdot \mathbf{S}_j)^2$, where \mathbf{S}_i is a spin-1 operator [5,13–28]. The biquadratic interaction works as a strong quantum fluctuation exchanging the spin-1 pairs, and kills the antisymmetric (dipolar) component. Since the biquadratic interaction is generally much smaller than the Heisenberg (bilinear) interaction [29], this spin nematics is hardly realized in materials. To have the latter bond nematics in a spin- $\frac{1}{2}$ model [6], often a very high magnetic field and a frustration effect are required. In a fully polarized spin- $\frac{1}{2}$ state, the standard lowest-energy excitation is an $S^z = -1$ magnon. However, if there are good reasons to suppress the kinetics of magnon, e.g., the frustration effect on a J_1 - J_2 square lattice model or a ring exchange model, the lowest excitation is replaced by the multimagnons propagating together [30–39]. For example, the bounded two-magnons consisting of two spin $\frac{1}{2}$ ’s pointing downward form a quadrupole by definition, and condense into a spin nematic phase near the saturation field in spin- $\frac{1}{2}$ ladders [35,36]. Whereas, in practice, it is hard to realize such a high field in experiments.

Recently, a double-layered spin- $\frac{1}{2}$ dimer system is proposed as a platform of spin nematics in a *zero magnetic field* [40]. When the spin $\frac{1}{2}$ ’s are antiferromagnetically coupled within the dimer, they form a singlet, and the interdimer Heisenberg interactions work as chemical potential and dope the $S = 1$ triplets. By the additional spin- $\frac{1}{2}$ four-body interdimer interaction, a biquadratic interaction between these doped $S = 1$ ’s is generated and two different types of spin nematic phases appear next to the singlet phase. The model based on the ferromagnetically coupled spin- $\frac{1}{2}$ dimers have

$S = 1$ triplet on a dimer bond by construction, and are also found to host a small window of spin nematic phase, when the second-order perturbative interdimer exchange coupling becomes relevant [41]. These works show that the spin nematics of the same type as that of the spin-1 BLBQ model is available in the spin- $\frac{1}{2}$ dimer systems by introducing the interdimer four-body exchanges which kill the antisymmetric part of the spin- $\frac{1}{2}$ wave function, like the biquadratic interaction does on spin 1.

In this paper, we replace the spin- $\frac{1}{2}$ dimer in Ref. [40] with spin-1 dimer, and deal with the two-dimensionally stacked spin-1 dimer forming a bilayer triangular lattice. We show that there are abundant types of magnetic and nonmagnetic long-range-ordered phases that are described by the quadrupolar as well as dipolar order parameters defined on a dimer bond. Considering a strong intradimer antiferromagnetic and biquadratic coupling, where maximally $S = 1$ moment ($S = 1$ is the on-bond spin-1 throughout the paper) is generated in each dimer out of two spin 1's, the original dimerized spin 1's degrees of freedom are transformed to an $S = 1$ hard-core boson. The interdimer Heisenberg spin exchange interaction is then transformed to the kinetic and pair fluctuation effect of these bosons as well as the magnetic exchange between $S = 1$'s. When the former fluctuation effect dominates, the $S = 1$ bosons lose their dipolar moment and condense, partially occupying the dimers as quadrupoles which we call ferroquadrupolar-BEC (FQ-BEC) phases. Besides, for a parameter region of nearly decoupled dimers, we find a spin nematic phase; we call "spin nematics" the phase based on the bound pairs of $S = 1$, typically found in spin-1 BLBQ model. In a dimer-based system, spin nematics can be realized when the bosons are fully packed on dimers. These quadrupolar phases are classified by the types of low-lying tower-of-state excitations in the energy spectrum that tell us how they break the symmetry. The richness of the phase diagram is possibly because of the large fluctuation of spin-1 moments allowed by the larger spin space compared to spin $\frac{1}{2}$'s since the former affords larger entanglement in constructing $S = 1$.

The technical aspect of this work is that, despite a seeming difficulty in increasing the degrees of freedom of the spin moments from spin $\frac{1}{2}$ to 1, one can treat it within a low-energy approximation using the same bosonic model as the spin- $\frac{1}{2}$ dimer case [40]. Aside from the transformation of the spin- $\frac{1}{2}$ model being exact, the only difference is how to map the interaction parameters of spin models to those of the bosonic model.

The direct motivation of dealing with spin-1 dimers instead of spin- $\frac{1}{2}$ dimers is to explain the intriguing magnetic properties of $\text{Ba}_3\text{MRu}_2\text{O}_9$ ($M = \text{Ca}, \text{Co}, \text{Ni}, \text{Cu}, \text{Zn}, \text{Sr}$) [42–47]. These materials are triangular lattice quantum magnets made up of dimerized Ru^{5+} ions that are expected to carry spin 1. While most of them exhibit conventional types of ordered phases such as singlet dimers or the antiferromagnet, the case of $M = \text{Zn}$ turned out to lack distinct signature of the phase transition, and remains nonmagnetic down to lowest temperature [42,43]. The possible correspondence between one of our FQ phases is to be finally discussed.

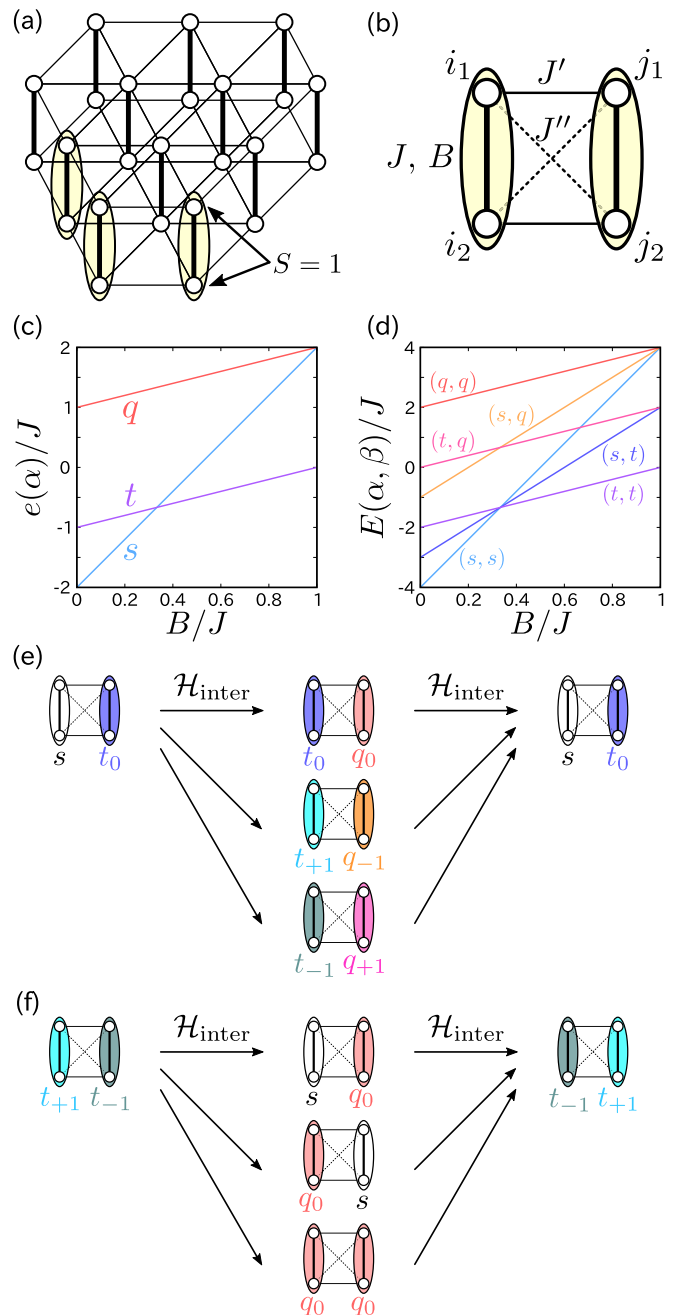


FIG. 1. (a) Schematic illustration of the spin-1 dimer model on a triangular lattice. (b) Intradimer and interdimer interactions, where $J > 0$, J' , J'' are the Heisenberg exchanges, and B is the biquadratic exchange. (c) Eigenenergy levels of $\mathcal{H}_{\text{intra}}$ of an isolated dimer. s , t , and q denote the singlet, triplet, and quintet states of the dimer, respectively. (d) Eigenenergy levels of $\mathcal{H}_{\text{intra}}$ of two isolated dimers without the interdimer J' and J'' . (e), (f) Examples of the second-order perturbation processes. Processes in (e) return to the original state $|s, t_0\rangle$. Processes in (f) exchange the $S^z = +1$ and -1 triplets, which are the origins of the biquadratic interactions between two triplets $(\mathcal{S}_i \cdot \mathcal{S}_j)^2$.

II. MODEL HAMILTONIAN

We consider a system consisting of dimers of two spin 1's. As shown in Fig. 1(a), the dimers stack parallelly and form a

double-layered triangular lattice. The Hamiltonian is given as

$$\begin{aligned}\mathcal{H} &= \mathcal{H}_{\text{intra}} + \mathcal{H}_{\text{inter}}, \\ \mathcal{H}_{\text{intra}} &= \sum_{i=1}^N [J\mathbf{S}_{i_1} \cdot \mathbf{S}_{i_2} + B(\mathbf{S}_{i_1} \cdot \mathbf{S}_{i_2})^2], \\ \mathcal{H}_{\text{inter}} &= \sum_{\langle i,j \rangle} \sum_{\gamma=1,2} (J'\mathbf{S}_{i_\gamma} \cdot \mathbf{S}_{j_\gamma} + J''\mathbf{S}_{i_\gamma} \cdot \mathbf{S}_{j_\gamma}),\end{aligned}\quad (1)$$

where \mathbf{S}_{i_γ} is the spin-1 operator of γ th site on an i th dimer. Here, we discriminate \mathbf{S}_{i_γ} defined on a lattice site from \mathbf{S}_i which is spin 1 defined on a dimer bond introduced in the next section. The summation $\langle i, j \rangle$ is taken over all the neighboring pairs of dimers, and $\bar{1} = 2$ and $\bar{2} = 1$. J (> 0) and B (> 0) denote the antiferromagnetic Heisenberg and the biquadratic interactions, respectively, J' and J'' are the interdimer Heisenberg interactions [Fig. 1(b)], and N is the number of dimers.

In Sec. III, we analyze the Hamiltonian (1) by transforming it to the effective model of the $S = 1$ bosons via the perturbation theory, and then solve it by the numerical exact diagonalization (ED) on a finite cluster. The magnetic properties of the model are described by the $S = 1$ carried by the hard-core boson.

To disclose the details of the phase diagram, particularly to fix the existence of the long-range order, we analyze the structure of the low-lying excited states, namely, a tower of states in Sec. IV. There, the spin-1 bosonic description is found to be not enough to understand several different classes of phases that form a quadrupolar ordering, which are classified as different types of ‘‘nematic’’ phases. We therefore introduce different operators defined on a dimer bond other than \mathbf{S}_i . To avoid confusion, we separate Sec. IV from Sec. III where the latter deals fully with the $S = 1$ bosonic description.

The classification of the above-mentioned different types of phases in comparison with the previously known phases based on quadrupolar moments is given in Sec. V, followed by a brief summary in Sec. VI.

III. EFFECTIVE $S = 1$ BOSONIC MODEL

A. Derivation of the effective Hamiltonian of bosons

1. Low-energy states of spin-1 dimers

Let us first consider an isolated dimer consisting of two spin 1 interacting via the BLBQ interactions $\mathcal{H}_{\text{BLBQ}} = J\mathbf{S}_1 \cdot \mathbf{S}_2 + B(\mathbf{S}_1 \cdot \mathbf{S}_2)^2$. The energy eigenstates of $\mathcal{H}_{\text{BLBQ}}$ are classified into singlet (s), triplets (t), and quintets (q), and their energies are given as $e(s) = -2J + 4B$, $e(t) = -J + B$, and $e(q) = J + B$, respectively. Figure 1(c) shows these energy levels as a function of B/J . At small B/J , the Heisenberg interaction is dominant and the lowest-energy state is a singlet. This singlet state is replaced by the triplet state when $B/J > \frac{1}{3}$, while the quintet cannot have lower energy than the triplet and remain as the excited states.

As a starting point of the perturbation, we take $\mathcal{H}_{\text{inter}} = 0$, where the ground state is the product state of the singlets on the isolated dimers for $B/J < \frac{1}{3}$, and that of triplets for $B/J > \frac{1}{3}$. In introducing $\mathcal{H}_{\text{inter}} \neq 0$, we consider the processes up to second order in J'/J and J''/J , so that the effective interactions between two adjacent dimers appear mainly in

the result. The energies of the disconnected two dimers with α and β multiplets $E(\alpha, \beta)$ are shown in Fig. 1(d). One can see that the states including quintets are higher in energy than the states without quintets when $B/J < \frac{2}{3}$. Therefore, based on the natural assumption that B/J is small enough, we construct the effective Hamiltonian for the low-energy manifold of states including only singlets and triplets.

The first-order process contributes to the energy correction of singlet and triplet states, as well as to the exchange of triplet and singlet on the neighboring two dimers. Within the second-order perturbation processes between two adjacent dimers, the intermediate excited states have at least one quintet as shown in the examples of the processes; in Fig. 1(e), the two-dimer state $|s, t_0\rangle$ returns to the same state through the excited states $|t_0, q_0\rangle$, $|t_{+1}, q_{-1}\rangle$, and $|t_{-1}, q_{+1}\rangle$, where $|s\rangle$ is the singlet state, and $|t_\mu\rangle$ and $|q_\mu\rangle$ are the triplet and the quintet states with $S^z = \mu$, respectively. In the processes shown in Fig. 1(f), $|t_{+1}, t_{-1}\rangle$, the two-dimer states with $S^z = +1$ and $S^z = -1$ triplet dimers, mixes with $|t_{-1}, t_{+1}\rangle$ via the three excited states $|s_0, q_0\rangle$, $|q_0, s_0\rangle$, and $|q_0, q_0\rangle$.

The low-energy basis can be described in the spin-1 hard-core bosonic language. The singlet corresponds to the vacuum, and the triplets are the bosons which are not allowed to doubly occupy a dimer. This kind of treatment is equivalent to the bond-operator approach, developed for the spin- $\frac{1}{2}$ dimer systems [48,49], and later applied to spin-1 dimer systems [50,51] and also to general spin- S dimers [52]. We choose the time-reversal-invariant form of the basis set $\{|t_{i,\alpha}\rangle\}$ described as

$$\begin{aligned}|t_{i,x}\rangle &= \frac{i}{2}(|+1, 0\rangle - |0, +1\rangle - |0, -1\rangle + |-1, 0\rangle), \\ |t_{i,y}\rangle &= \frac{1}{2}(|+1, 0\rangle - |0, +1\rangle + |0, -1\rangle - |-1, 0\rangle), \\ |t_{i,z}\rangle &= -\frac{i}{\sqrt{2}}(|+1, -1\rangle - |-1, +1\rangle),\end{aligned}\quad (2)$$

where the dimer states on the right-hand side described as $|S_{i_1}^z, S_{i_2}^z\rangle$ are those classified by the S^z values of the two spins forming a dimer. The details of the bond-operator approach and the description of the original spin operators using the bosonic operators are shown in Appendix A 1.

2. Effective Hamiltonian

The triplet state with α component $|t_{i,\alpha}\rangle$ at site i is expressed as $b_{i,\alpha}^\dagger |0\rangle$, where $|0\rangle$ is the singlet state and $b_{i,\alpha}^\dagger$ is the creation operator of a boson representing that triplet. Using this bosonic operator, the effective Hamiltonian \mathcal{H}_{eff} up to second order in J'/J and J''/J is given as

$$\begin{aligned}\mathcal{H}_{\text{eff}} &= E_0 + \mathcal{H}_\mu + \mathcal{H}_t + \mathcal{H}_p + \mathcal{H}_V + \mathcal{H}_J + \mathcal{H}_B + \mathcal{H}_{3\text{body}}, \\ \mathcal{H}_\mu &= -\mu \sum_{i=1}^N n_i, \quad \mathcal{H}_t = t \sum_{\langle i,j \rangle} \sum_{\alpha=x,y,z} b_{i,\alpha}^\dagger b_{j,\alpha} + \text{H.c.}, \\ \mathcal{H}_p &= P \sum_{\langle i,j \rangle} \sum_{\alpha=x,y,z} b_{i,\alpha}^\dagger b_{j,\alpha}^\dagger + \text{H.c.}, \quad \mathcal{H}_V = V \sum_{\langle i,j \rangle} n_i n_j, \\ \mathcal{H}_J &= J \sum_{\langle i,j \rangle} \mathbf{S}_i \cdot \mathbf{S}_j n_i n_j, \quad \mathcal{H}_B = B \sum_{\langle i,j \rangle} (\mathbf{S}_i \cdot \mathbf{S}_j)^2 n_i n_j.\end{aligned}\quad (3)$$

Here, $n_i = \sum_{\alpha} b_{i,\alpha}^{\dagger} b_{i,\alpha}$ is the number operator, and the hard-core condition $n_i = 0$ or 1 is imposed on the number operator. The spin-1 operator of i th boson is expressed by \mathcal{S}_i , where $\mathcal{S}_i^{\alpha} = -i \sum_{\beta,\gamma} \varepsilon_{\alpha\beta\gamma} b_{i,\beta}^{\dagger} b_{i,\gamma}$ and $\varepsilon_{\alpha\beta\gamma}$ is the Levi-Civita symbol. We note that the Hamiltonian keeps the SU(2) symmetry of triplets [40,53,54], as far as the magnetic field is not applied [55].

The parameters included in \mathcal{H}_{eff} are described by the original interaction parameters in Eq. (1) as

$$\begin{aligned} E_0 &= (-2J + 4B)N, \\ \mu &= -J + 3B + \frac{20z}{27(J-B)}(J' - J'')^2, \\ t &= \frac{4}{3}(J' - J''), \quad P = -\frac{4}{3}(J' - J''), \\ V &= \left[\frac{40}{27(J-B)} - \frac{8}{9(J+3B)} - \frac{2}{9J} \right] (J' - J'')^2, \\ \mathcal{J} &= \frac{J' + J''}{2} + \left[-\frac{4}{3(J+3B)} + \frac{1}{12J} \right] (J' - J'')^2, \\ \mathcal{B} &= \left[-\frac{4}{9(J+3B)} - \frac{1}{144J} \right] (J' - J'')^2, \end{aligned} \quad (4)$$

where z is the coordination number. One can immediately see that μ , t , P , and \mathcal{J} terms include the terms that originate from the first-order process, whereas V and \mathcal{B} terms do not.

There are some processes at the second-order level where the three dimers take part in, which we denote as $\mathcal{H}_{3\text{body}}$ in Eq. (3). We numerically evaluate the effects of $\mathcal{H}_{3\text{body}}$ on the effective Hamiltonian by comparing the energies of the ground states of the original Hamiltonian \mathcal{H} [Eq. (1)], and of the effective Hamiltonian \mathcal{H}_{eff} [Eq. (3)] with and without $\mathcal{H}_{3\text{body}}$ in a small cluster, finding that it does not play a significant role. We thus discard this $\mathcal{H}_{3\text{body}}$ term in the following for simplicity. The details of the evaluation of the effective model are shown in Appendix A 2. We further show that even the other second-order terms included in Eq. (3) do not contribute much to the majority of phases we deal with. The way how the interdimer interactions work thus turns out to be simple.

3. Physical quantities

For the analysis of the effective model, we calculate the following properties that characterize the ground state. The boson density per dimer is denoted as $\langle n_t \rangle = N^{-1} \sum_{i=1}^N \langle n_i \rangle$, and its structure factor is given as

$$N(\mathbf{k}) = \frac{1}{N} \sum_{i,j=1}^N \langle n_i n_j \rangle e^{i\mathbf{k} \cdot (\mathbf{r}_i - \mathbf{r}_j)}. \quad (5)$$

The magnetic properties are examined by the spin and quadrupole structure factors

$$\mathcal{S}(\mathbf{k}) = \frac{1}{N} \sum_{i,j=1}^N \langle \mathcal{S}_i \cdot \mathcal{S}_j n_i n_j \rangle e^{i\mathbf{k} \cdot (\mathbf{r}_i - \mathbf{r}_j)}, \quad (6)$$

$$\mathcal{Q}(\mathbf{k}) = \frac{1}{N} \sum_{i,j=1}^N \langle \mathcal{Q}_i \cdot \mathcal{Q}_j n_i n_j \rangle e^{i\mathbf{k} \cdot (\mathbf{r}_i - \mathbf{r}_j)}, \quad (7)$$

where \mathcal{Q}_i is the five-component vector representation of quadrupole operator of spin-1 bosons defined as

$$\mathcal{Q}_i = \begin{pmatrix} \mathcal{Q}_i^{x^2-y^2} \\ \mathcal{Q}_i^{3z^2-r^2} \\ \mathcal{Q}_i^{xy} \\ \mathcal{Q}_i^{yz} \\ \mathcal{Q}_i^{zx} \end{pmatrix} = \begin{pmatrix} (\mathcal{S}_i^x)^2 - (\mathcal{S}_i^y)^2 \\ \frac{1}{\sqrt{3}} [3(\mathcal{S}_i^z)^2 - \mathcal{S}(\mathcal{S}+1)] \\ \mathcal{S}_i^x \mathcal{S}_i^y + \mathcal{S}_i^y \mathcal{S}_i^x \\ \mathcal{S}_i^y \mathcal{S}_i^z + \mathcal{S}_i^z \mathcal{S}_i^y \\ \mathcal{S}_i^z \mathcal{S}_i^x + \mathcal{S}_i^x \mathcal{S}_i^z \end{pmatrix}. \quad (8)$$

In a system with spin 1 defined on each site, typically represented by the spin-1 BLBQ models, the quadrupole operator \mathcal{Q}_i is the ‘‘onsite’’ operator. For a system with spin $\frac{1}{2}$ per site, the quadrupole operator is defined on a bond instead since one needs to prepare a spin 1 from two spin $\frac{1}{2}$'s [32,56]. In the present case, the two sites forming a dimer each host spin-1 operators \mathcal{S}_{i_1} and \mathcal{S}_{i_2} , and \mathcal{S}_i , which is defined on a dimer bond, is a composition of these two spin 1's. For this reason, one can also define another quadrupole operator on dimer bond as

$$\mathcal{Q}_{i_{12}}^{\alpha\beta} = \mathcal{S}_{i_1}^{\alpha} \mathcal{S}_{i_2}^{\beta} + \mathcal{S}_{i_1}^{\beta} \mathcal{S}_{i_2}^{\alpha} - \frac{2}{3} (\mathcal{S}_{i_1} \cdot \mathcal{S}_{i_2}) \delta_{\alpha\beta}. \quad (9)$$

Then, one finds that $\mathcal{Q}_{i_{12}}$ and \mathcal{Q}_i are equivalent in terms of our triplet states, namely,

$$\langle t_{\alpha} | \mathcal{Q}_{i_{12}}^{\mu\nu} | t_{\beta} \rangle = \langle t_{\alpha} | \mathcal{Q}_i^{\mu\nu} | t_{\beta} \rangle \quad (10)$$

holds for $\alpha, \beta, \mu, \nu = x, y, z$. In the same manner, the spin operator inside i th spin-1 dimer defined as

$$\mathcal{S}_{i_{12}}^{\alpha} = \mathcal{S}_{i_1}^{\alpha} + \mathcal{S}_{i_2}^{\alpha} \quad (11)$$

works in the same way as \mathcal{S}_i^{α} for the triplet states, i.e.,

$$\langle t_{\alpha} | \mathcal{S}_{i_{12}}^{\mu} | t_{\beta} \rangle = \langle t_{\alpha} | \mathcal{S}_i^{\mu} | t_{\beta} \rangle \quad (12)$$

holds for $\alpha, \beta, \mu = x, y, z$.

Unlike the spin-1 BLBQ models [18], the number of spin-1 bosons per dimer is not fixed in our Hamiltonian. However, one can consider the spin-1 BLBQ model as the $\langle n_t \rangle = 1$ limiting case of our model since the two models share the same definition, Eq. (8). One can thus make use of the analysis applied to the spin-1 BLBQ model [18]; there are so-called SU(3) points in the BLBQ model, where the three components of \mathcal{S} and the five components of \mathcal{Q} equivalently form the eight elements of the SU(3) Lie algebra. Exactly at this point the transition between the magnetic and the spin nematic or quadrupolar phases is known to take place. Numerically, this transition is identified by the point where $\mathcal{S}(\mathbf{k})$ and $\tilde{\mathcal{Q}}(\mathbf{k}) \equiv (3/5)\mathcal{Q}(\mathbf{k})$ take the same values. We thus use this normalized value $\tilde{\mathcal{Q}}(\mathbf{k})$ to determine the phase transitions between the magnetic and the quadrupolar states.

B. Results of the $\mathcal{S} = 1$ bosonic model

1. Phase diagram

We numerically diagonalize \mathcal{H}_{eff} on the $N = 12$ triangular lattice ($z = 6$) under the periodic boundary condition. The phase diagrams on the plane of J'/J and J''/J at $B/J = 0.2$ and 0.4 are shown in Figs. 2(a) and 2(b).

The phase diagram is divided into four parts overall. When $J' \sim J'' > 0$, the antiferromagnetic phases with

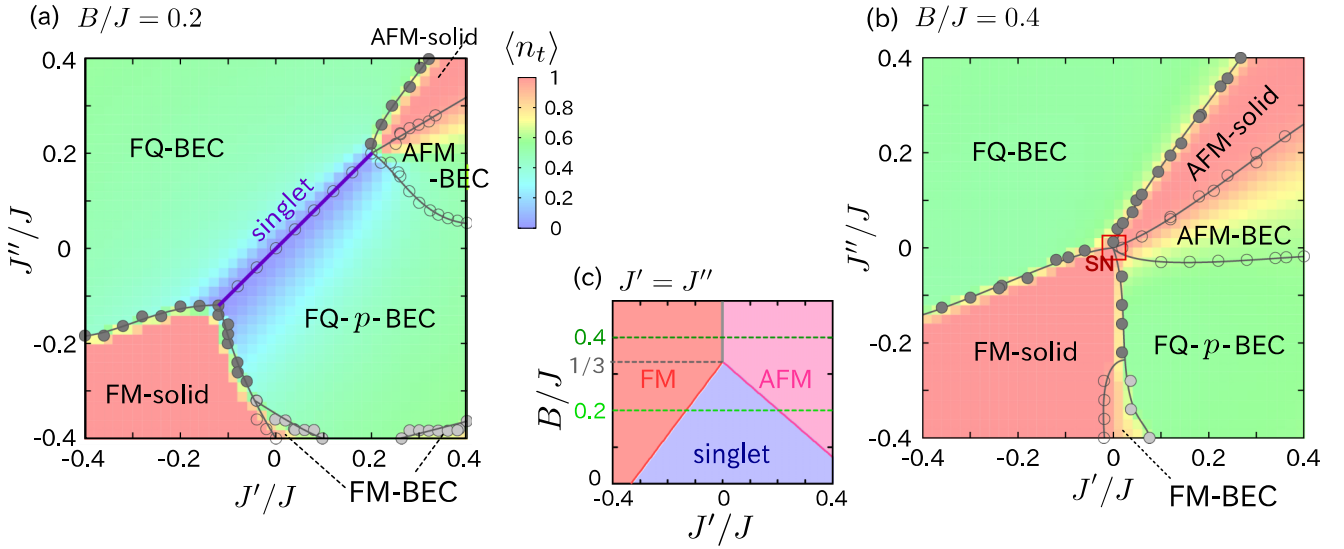


FIG. 2. Ground-state phase diagram of the spin-1 dimer triangular lattice at (a) $B/J = 0.2$ and (b) 0.4 , obtained by the numerical diagonalization of the effective model with $N = 12$. Filled and open circles represent the first- and second-order phase transitions, where the transition between FM-BEC and FQ- p -BEC is weakly first order. FM, AFM, FQ represent the ferromagnetic, antiferromagnetic, and ferroquadrupolar phases, and $\langle n_t \rangle \approx 1$ and $\lesssim 0.9$ are the solid and BEC states of bosons. Colors in the phase diagram are the density plot of the triplet number $\langle n_t \rangle$. The small J', J'' region marked with red square in (b) encloses the spin nematic (SN) phase [see Fig. 8(b)]. (c) Phase diagram on the plane of J'/J and B/J , whose fixed B/J lines correspond to the $J' = J''$ line of the phase diagrams in (a) and (b).

$\langle n_t \rangle \approx 1$ (AFM-solid) and $\langle n_t \rangle \lesssim 0.9$ (AFM-BEC) are stabilized by the antiferromagnetic interaction $\mathcal{J} > 0$ between bosons occupying the neighboring dimers. On the opposite part of the phase diagram, $J' \sim J'' < 0$, the ferromagnetic phase with $\langle n_t \rangle \approx 1$ (FM-solid) is realized for similar reasons. When $J' - J'' < 0$ and $J' - J'' > 0$, two different types of ferroquadrupolar phases, FQ-BEC and FQ- p -BEC, appear over a wide parameter region. Throughout both of the phase diagrams, we see no particular features of bosons, i.e., $N(\mathbf{k})$ takes the maximum value at Γ point, which indicates that bosons distribute uniformly in space and do not show any translational symmetry-breaking long-range order.

The phase boundaries are determined from two aspects: whether the bosons are fully occupied and form a quantum spin-1 system (solid) with $\langle n_t \rangle = 1$ or become a BEC with $\langle n_t \rangle < 1$, and what kind of magnetic correlations they have in terms of $\mathcal{S}(\mathbf{k})$ or $\mathcal{Q}(\mathbf{k})$. The absolute values of $\mathcal{S}(\mathbf{k})$ or $\mathcal{Q}(\mathbf{k})$ depend on the bosonic density $\langle n_t \rangle$, but their spatial modulations originate from the purely magnetic ones since $\langle n_t \rangle$ is spatially uniform, as we see shortly. These boundaries are basically second-order phase transitions, and existence of the long-range order is examined precisely in Sec. IV.

2. $J' = J''$ line

The starting point is $J' = J'' = 0$, at which the ground state is the product state of the isolated-dimer state. As one can see from Eq. (4), most of the parameters, namely, t, P, V, B , are the linear or the square functions of $(J' - J'')$. Therefore, these parameters remain zero exactly at $J' = J''$, namely, the interdimer interactions cancel out because of the geometrical frustration effect.

In fact, when $B/J = 0.2$, the singlet product state, namely $\langle n_t \rangle = 0$, remains a ground state along this line. The end point

of this singlet phase is evaluated in the following manner; when $J' = J''$, the effective Hamiltonian consists only of two terms

$$\mathcal{H}_{J'=J''} = -\mu \sum_{i=1}^N n_i + \mathcal{J} \sum_{\langle i,j \rangle} \mathcal{S}_i \cdot \mathcal{S}_j n_i n_j, \quad (13)$$

with $\mu = -J + 3B$ and $\mathcal{J} = J'$. Regardless of its sign, \mathcal{J} works as an effective attractive interaction between bosons since it is energetically favorable to occupy the neighboring pairs of dimers with triplets to gain the magnetic interaction energy. Then, there is a first-order transition between the $\langle n_t \rangle = 0$ singlet and the $\langle n_t \rangle = 1$ FM or AFM solid phases. The phase boundary can be obtained by comparing their energies $E_0(N)$ and $E_1(N)$, where there is a relationship

$$E_1(N) = E_0(N) - \mu N + 3N e_{\text{bond}}. \quad (14)$$

Here, e_{bond} is evaluated as the bond energy of the ground state of the spin-1 triangular lattice Heisenberg model $J' \sum_{\langle i,j \rangle} \mathcal{S}_i \cdot \mathcal{S}_j$ for $N = 12$. Figure 2(c) shows the resultant phase diagram on the plane of $J' = J''$ and B with $J = 1$. The singlet phase corresponding to the straight line in Fig. 2(a) shrinks toward smaller $J' = J''$ value with increasing B/J , and disappears at $B/J = \frac{1}{3}$. For $B/J > \frac{1}{3}$, $\langle n_t \rangle = 1$ is realized throughout the whole $J' = J''$ line. The singlet phase in the phase diagram of $B/J = 0.2$ spans over a finite range of $|J' - J''|$, which is to be confirmed in the instability analysis in Sec. V A.

3. Ferromagnetic and antiferromagnetic phases

The FM and AFM phases extend from the end points of the $J' \simeq J''$ singlet phase discussed above. In Fig. 3, we show the total energy divided by N , e_{all} , and the contributions from each of the terms $e_t, e_P, e_{\mathcal{J}}$, and e_B , the boson density $\langle n_t \rangle$, and the values of the structure factors at Γ, K , and M

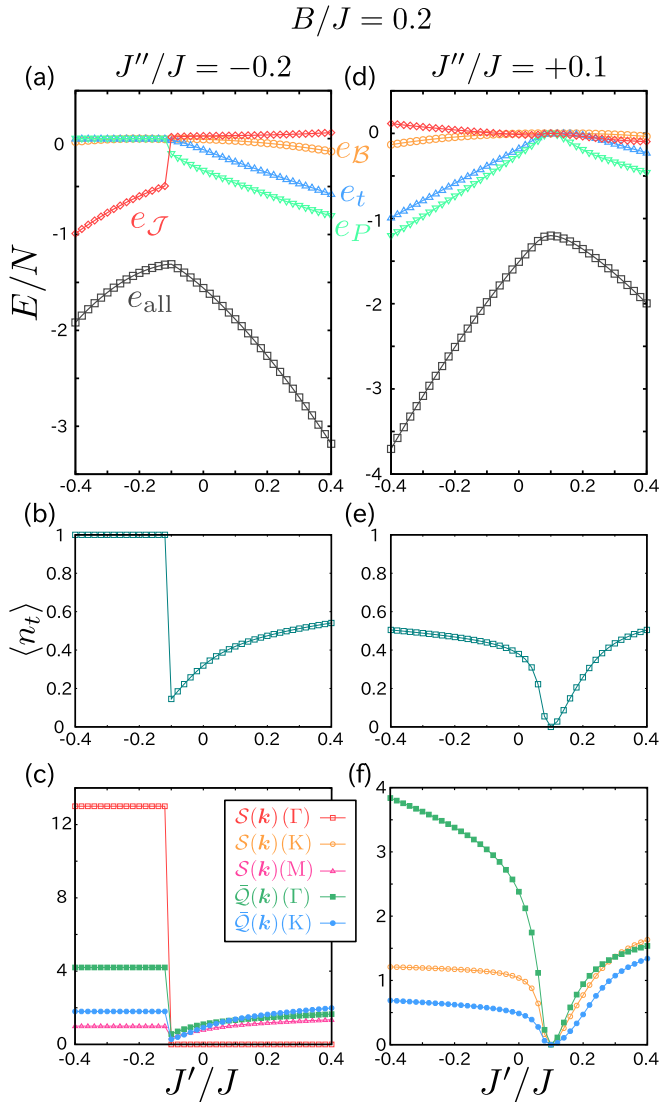


FIG. 3. J'/J dependencies of the physical quantities at $B/J = 0.2$ when (a)–(c) $J''/J = -0.2$ and (d)–(f) $J''/J = +0.1$. (a), (d) Total energies e_{all} and the contributions from major terms in the effective Hamiltonian e_t , e_P , $e_{\mathcal{J}}$, and e_B . (b), (e) Triplet densities $\langle n_t \rangle$. (c), (f) Spin [Eq. (6)] and quadrupole [Eq. (7)] structure factors at Γ , K, M points in the reciprocal space. Quadrupole structure factors denoted as $\tilde{Q}(\mathbf{k})$ are normalized to be compared with the spin structure factors $S(\mathbf{k})$ (see Sec. III A 3 for details).

points of the Brillouin zone. We vary J'/J along the fixed $J''/J = -0.2$ and 0.1 lines. In the former case, a jump in the physical quantity is found at the transition from the FM-solid to the FQ- p -BEC phase. Compared to other phases, the FM-solid phase has a large energy gain of $e_{\mathcal{J}}$, indicating that the magnetic interaction \mathcal{J} is responsible for stabilizing the FM-solid. Indeed, $S(\mathbf{k})$ shows a peak at the Γ point in this phase while the other $S(\mathbf{k})$ and $Q(\mathbf{k})$ remain small. When we vary J'/J along $J''/J = 0.1$ [Figs. 3(d)–3(f)], $\langle n_t \rangle \lesssim 0.55$, and the system remains a BEC. The transitions along this line are of second order. At $J'/J \gtrsim 0.3$, $S(\mathbf{k})$ at K point starts to overwhelm $Q(\mathbf{k})$ at the Γ point which we recognize as the AFM-BEC phase, following the treatment in Ref. [18] (see

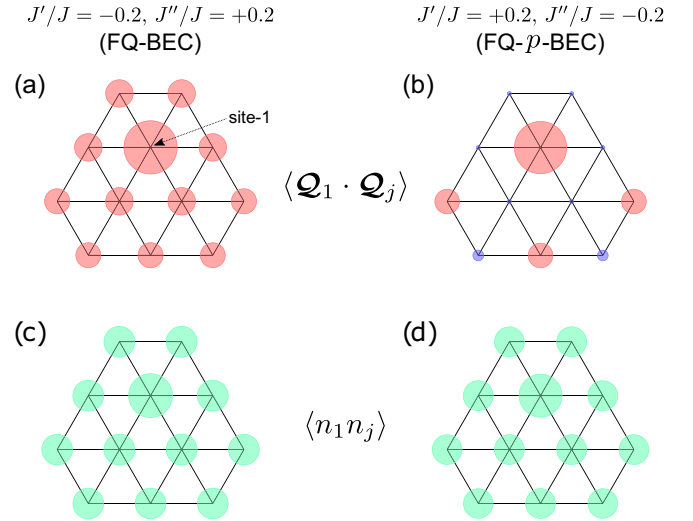


FIG. 4. Spatial correlation functions for $(J'/J, J''/J) = (-0.2, +0.2)$ in FQ-BEC and $(+0.2, -0.2)$ in FQ- p -BEC phases at $B/J = 0.2$: the quadrupolar correlations in (a), (b) $\langle \mathcal{Q}_1 \cdot \mathcal{Q}_j \rangle$ and the boson-boson correlation in (c), (d) $\langle n_1 n_j \rangle$. Areas of the circles are proportional to the amplitude of correlations $|\langle \mathcal{Q}_1 \cdot \mathcal{Q}_j \rangle|$ or $|\langle n_1 n_j \rangle|$. Red and blue circles in (a) and (b) correspond to the signs of $\langle \mathcal{Q}_1 \cdot \mathcal{Q}_j \rangle$, positive and negative, respectively.

the last part of Sec. III A 3). The phase boundaries in Fig. 2 are classified into first- and second-order ones (filled and open circles) according to this analysis.

4. FQ phases

In the phase diagram, there are two different ferro-quadrupolar phases, FQ-BEC extending at $J'' > J'$ and FQ- p -BEC at $J'' < J'$. As we see in Figs. 3(e) and 3(f), $\langle n_t \rangle$ and $Q(\mathbf{k})$ both decrease down to zero at the boundary of the two phases where the singlet state appears, which marks the second-order transition. In such a case, the order parameters of the two phases should differ. In fact, although $Q(\mathbf{k})$ at the Γ point is dominant in both phases, only in the FQ- p -BEC phase $Q(\mathbf{k})$ at the K point takes as large value.

Figures 4(a) and 4(b) show the two-point quadrupole correlations between site 1 and site j , $\langle \mathcal{Q}_1 \cdot \mathcal{Q}_j \rangle$, in FQ-BEC and FQ- p -BEC phases. The former correlation develops uniformly in space, whereas in the latter, there is apparently a growth of correlation in the period of twice the lattice spacing in all three directions. This three-sublattice-like structure of quadrupole moments corresponds to the peak of $Q(\mathbf{k})$ at the K point. Figures 4(c) and 4(d) are the two-point correlation of bosons, $\langle n_1 n_j \rangle$, which are both uniform in space. This indicates that the three-sublattice structure of the quadrupolar moment in the FQ- p -BEC is not because of the modulated bosonic distribution but originates purely from the correlation between the spin degrees of freedom S_i ; the nearest-neighbor quadrupolar correlation is suppressed, while the next nearest-neighbor correlations are ferroic.

5. Case of $B/J = 0.4$

We now focus on the case of $B/J = 0.4$, where μ takes a positive value. The singlet phase no longer exists and

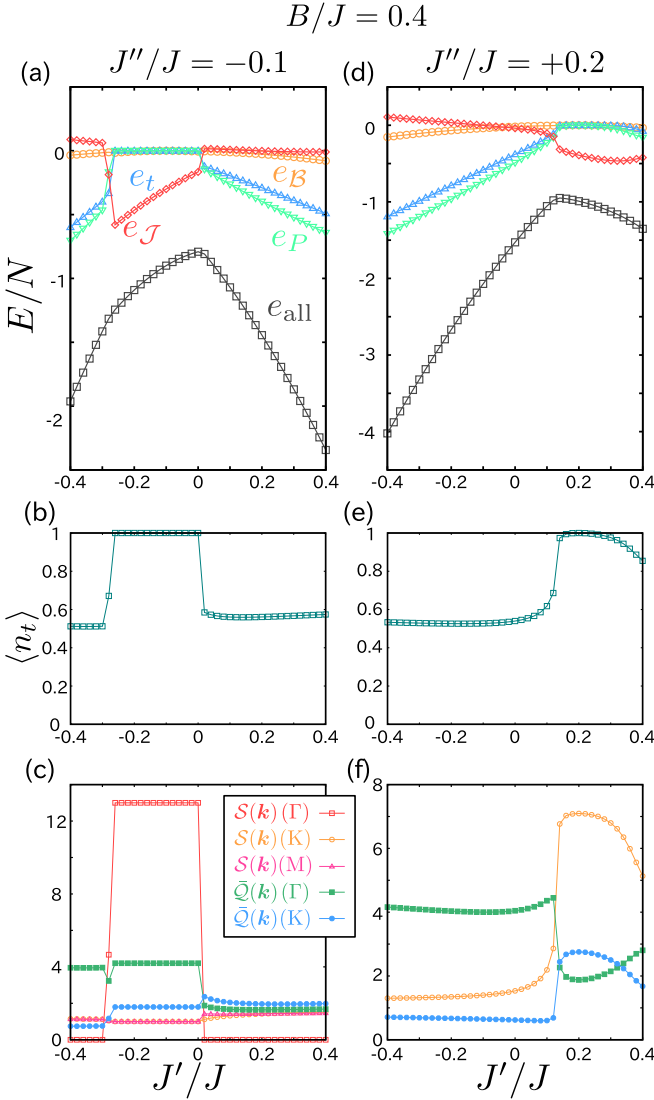


FIG. 5. J'/J dependence of the physical quantities at $B/J = 0.4$ when (a)–(c) $J''/J = -0.1$ and (d)–(f) $J''/J = +0.2$. (a), (d) Total energies e_{all} and the contributions from major terms in the effective Hamiltonian e_t , e_p , e_J , and e_B . (b), (e) Triplet densities $\langle n_t \rangle$. (c), (f) Spin [Eq. (6)] and quadrupole [Eq. (7)] structure factors at Γ , K, M points in the reciprocal space. Quadrupole structure factors denoted as $\tilde{Q}(\mathbf{k})$ are normalized to be compared with the spin structure factors $S(\mathbf{k})$ (See Sec. III A 3 for details).

the triplet product state realized at $J' = J'' = 0$ immediately transforms to either of the phases we discussed earlier when the interdimer interactions become finite. Figure 5 shows the J'/J dependencies of energies, boson density, and the structure factors to be compared with Fig. 3. The first-order transitions separating the FM-solid from FQ phases are observed. The boson density in the FQ-BEC phase remains quite stable at around $\langle n_t \rangle \approx 0.55$, indicating that the nature of the BEC phases does not change much with B/J .

6. Orders of perturbation

The interaction parameters in Eq. (4) include the first- and second-order terms. Among them, V and B disappear

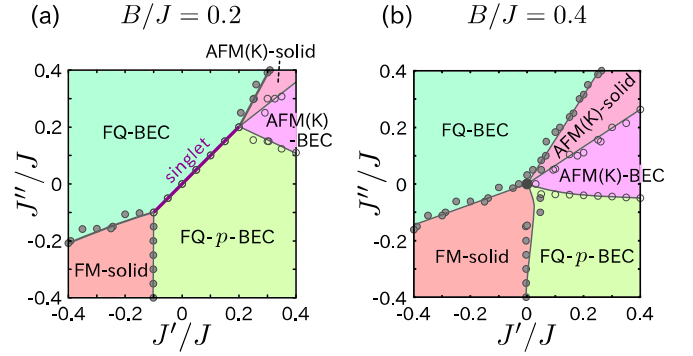


FIG. 6. (a), (b) Phase diagrams of the effective model up to the first order in J'/J and J''/J at (a) $B/J = 0.2$ and (b) $B/J = 0.4$, obtained by the analysis of the results of the numerical diagonalization on the $N = 12$ cluster.

when we neglect the second-order terms. To see how much the second-order terms contribute to the determination of the phase diagram, we perform the numerical diagonalization by limiting the parameter values to those up to the first order in J'/J and J''/J with $N = 12$. Figures 6(a) and 6(b) show the phase diagrams at $B/J = 0.2$ and 0.4 . The phase diagrams are in good agreement with those in Figs. 2(a) and 2(b), indicating that V and B do not play a major role in the five representative phases FM-solid, AFM-solid/BEC, FQ-BEC, and FQ- p -BEC.

IV. LONG-RANGE ORDERS OF MULTIPLE QUADRUPOLAR PHASES

We so far disclosed the overall magnetic properties of the system in the $S = 1$ bosonic description based on the $N = 12$ ED. In general, the ED results suffer from a serious finite-size effect, which however does not apply to this study. One of the authors has previously analyzed the same bosonic Hamiltonian (3) for the spin- $\frac{1}{2}$ dimer model with $N = 12$ ED, and showed that the phase boundaries are quantitatively in good agreement with the analytical ones at $N = \infty$ [40]. The remaining issue is to explicitly show the existence of long-range FQ, AFM, and FM orderings, which is done by the Anderson tower analysis known to be valid for ED with small clusters [57]. For that purpose, we perform the thick-restart Lanczos method [58] and disclose the scaling properties of the low-lying levels of the exact spectra. The emergent quasidegenerate joint states (QDJS) at the lowest-energy levels that are linear with respect to $S(S + 1)$ indicate the existence of SU(2) symmetry-broken long-range order [59–61]. For example, the ferromagnetically ordered moments represented by a rigid body of uniaxial rotator exhibit the QDJS with only one level in each S sector all belonging to the Γ point. The 120° Néel ordering of triangular lattice antiferromagnet is the biaxial rotator or a quantum top [60,61], which gives the $(2S + 1)$ -degenerate levels forming QDJS. The slope of the QDJS is proportional to $1/N$, and when $N \rightarrow \infty$, they collapse into degenerate manifold of ground states that signal the symmetry breaking. In the following analysis, we confirmed it by comparing with the $N = 9$ QDJS.

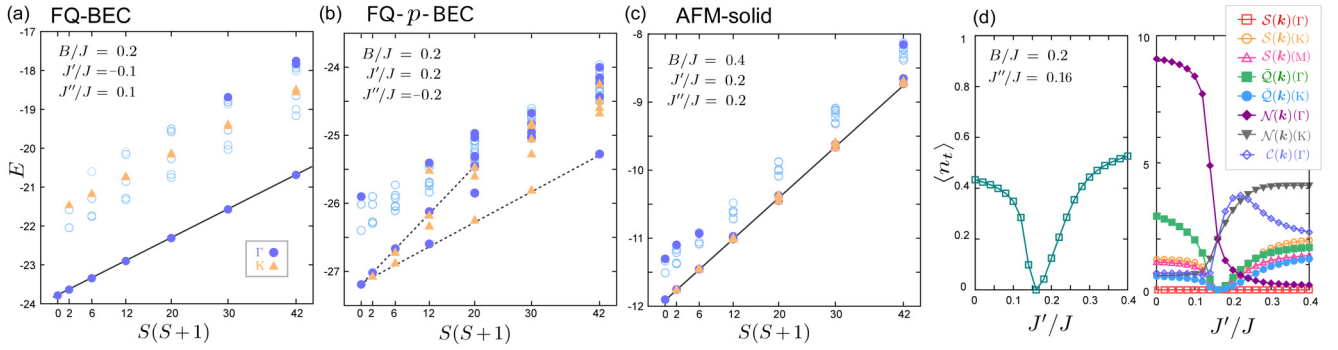


FIG. 7. Low-energy excited states as a function of $S(S+1)$ for (a) FQ-BEC, (b) FQ- p -BEC, (c) AFM-solid phases for $N = 12$ cluster. Filled circles and triangles are the Γ and K points of the Brillouin zone and open circles are from the other \mathbf{k} points. Those following the solid line are tower of states indicating the long-range order. (d) Triplet density (left) and structure factors at Γ , K points (right), including $\mathcal{N}(\mathbf{k})$ and $\mathcal{C}(\mathbf{k})$ which gives the information on the details of the magnetic properties of the dimerized spin $S_{i\gamma}$. J'/J is varied from FQ-BEC ($J'/J < 0.15$), FQ- p -BEC ($0.15 < J'/J < 0.25$) to AFM-BEC phases.

Figures 7(a)–7(c) show the ones from the FQ-BEC, FQ- p -BEC, and AFM-solid phases, respectively. For the (a) FQ-BEC and (c) AFM-solid phases, we clearly find QDJS marked with solid lines. The QDJS in Fig. 7(a) consists of $S = 0, 1, 2, 3, \dots$ states with only one level in each S sector, all belonging to the Γ point, characterizing the excitation of the U(1) uniaxial rotator. They clearly differ from the one known for the spin-1 nematic (ferroquadrupolar) phase, where the low-lying states consist of even- S sectors with Γ points [56] [cf. see Fig. 8(a) of the SN phase]. This indicates that the order parameter $\mathcal{Q}_i^{\alpha\beta}$ alone is not enough to physically classify multiple quadrupolar phases of dimer systems. Indeed, the quadrupolar moment on a dimer bond is decomposed as

$$\mathcal{Q}_i^{\alpha\beta} = - \left\{ \frac{3}{4} [(q_i^\alpha q_i^\beta + p_i^\alpha p_i^\beta) + (q_i^\beta q_i^\alpha + p_i^\beta p_i^\alpha)] - \frac{2}{3} \delta_{\alpha\beta} \right\} n_i, \quad (15)$$

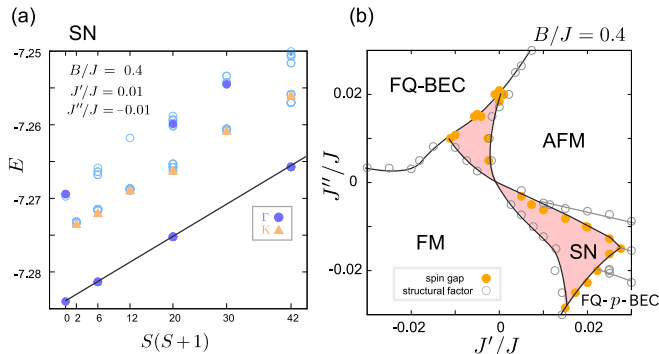


FIG. 8. (a) Low-energy excited states as a function of $S(S+1)$ at $J'/J = 0.01$ and $J''/J = -0.01$, $B/J = 0.4$. (b) Phase diagram at small J'/J and J''/J and $B/J = 0.4$ determined by the Anderson tower analysis, which is the magnification of the region indicated by red square at the center part of Fig. 2(c). SN phase is found for $J' \sim -J'$, where the lowest excited state is $S = 2$. The boundaries are given both from the crossing of $S = 1, 2$ levels (filled circle) and from the structural factor (open circle). Physical quantities along the fixed $J''/J = 0.01$ line in the phase diagram are given in Fig. 12.

using the internal degrees of freedom of a dimer [54], namely, the staggered operator of the two spins and the vector chiral operator

$$\mathbf{q}_i = \frac{1}{2}(\mathbf{S}_{i_1} - \mathbf{S}_{i_2}), \quad (16)$$

$$\mathbf{p}_i = \mathbf{S}_{i_1} \times \mathbf{S}_{i_2}. \quad (17)$$

These operators are related to our $\mathcal{S} = 1$ bosonic operator as $b_{i,\alpha} \propto q_i^\alpha - ip_i^\alpha$ and $b_{i,\alpha}^\dagger \propto q_i^\alpha + ip_i^\alpha$. When at least $\langle \mathbf{q}_i \rangle \neq \mathbf{0}$ or $\langle \mathbf{p}_i \rangle \neq \mathbf{0}$ is fulfilled, we have $\langle \mathcal{Q}_i \rangle \neq \mathbf{0}$, whereas the vice versa does not always hold. The structural factors of \mathbf{q}_i and \mathbf{p}_i are

$$\mathcal{N}(\mathbf{k}) = \frac{1}{N} \sum_{i,j=1}^N \langle \mathbf{q}_i \cdot \mathbf{q}_j \rangle e^{i\mathbf{k} \cdot (\mathbf{r}_i - \mathbf{r}_j)}, \quad (18)$$

$$\mathcal{C}(\mathbf{k}) = \frac{1}{N} \sum_{i,j=1}^N \langle \mathbf{p}_i \cdot \mathbf{p}_j \rangle e^{i\mathbf{k} \cdot (\mathbf{r}_i - \mathbf{r}_j)}. \quad (19)$$

The classification of quadrupolar phases in terms of these order parameters is given in Table I. The conventional SN phase found in the BLBQ has $\langle \mathcal{Q}_i \rangle \neq \mathbf{0}$ and with other magnetic order parameters absent, and occurs only when $\langle n_i \rangle = 1$. Here, $\langle \mathcal{Q}_i \rangle \neq \mathbf{0}$ is not supported by $\langle \mathbf{q}_i \rangle \neq \mathbf{0}$ or $\langle \mathbf{p}_i \rangle \neq \mathbf{0}$, but by $\langle q_i^\alpha q_i^\beta \rangle \neq 0$ or $\langle S_{i_1}^\alpha S_{i_1}^\beta \rangle \neq 0$. For $\langle \mathbf{p}_i \rangle \neq \mathbf{0}$ and $\langle \mathbf{q}_i \rangle = \langle \mathcal{S}_i \rangle = \mathbf{0}$, the vector chirality degrees of freedom condenses and forms a nematic order, again suppressing all types of magnetic orderings. This phase is called the p -nematic phase and is distinguished from the n -nematic phase (SN). In the SN

TABLE I. Classification of multiple phases by the order parameters \mathbf{q} , \mathbf{p} , \mathcal{S} , \mathcal{Q} , and solid (S) or liquid (L) type boson distributions. FQ-BEC corresponds to F-nematic in Ref. [54].

Phases	$\langle \mathbf{q} \rangle$	$\langle \mathbf{p} \rangle$	$\langle \mathcal{S} \rangle$	$\langle \mathcal{Q} \rangle$	Boson
SN (n -nematic)	$\mathbf{0}$	$\mathbf{0}$	$\mathbf{0}$	$\neq \mathbf{0}$	S
Chiral (p -nematic)	$\mathbf{0}$	$\neq \mathbf{0}$	$\mathbf{0}$	$\neq \mathbf{0}$	L
FM	$\mathbf{0}(S)$ or $\neq \mathbf{0}(L)$	$\mathbf{0}$	$\neq \mathbf{0}$	$\neq \mathbf{0}$	S or L
AFM	$\mathbf{0}(S)$ or $\neq \mathbf{0}(L)$	$\neq \mathbf{0}$	$\neq \mathbf{0}$	$\neq \mathbf{0}$	S or L
FQ-BEC	$\neq \mathbf{0}$	$\mathbf{0}$	$\mathbf{0}$	$\neq \mathbf{0}$	L

phase, the tower-of low-lying states consist only of multiple S_{tot} sectors in units of two or three bosons since only the multi-boson bound states are allowed as quasiparticles. Whereas, in the p -nematic phase, typical magnon excitations are allowed and the tower of states consists of all S_{tot} sectors.

The standard magnetic phases, AFM and FM, are based on $\langle \mathcal{S}_i \rangle \neq \mathbf{0}$. The FQ-BEC phase has $\langle \mathbf{q}_i \rangle \neq \mathbf{0}$ and $\langle \mathbf{p}_i \rangle = \mathbf{0}$, where the small moments induced on the dimerized two spins are always forming an antiparallel state and *keep the dimer unit always nonmagnetic* as $\langle \mathcal{S}_i \rangle = \mathbf{0}$. The small moments form a magnetic long-range order inside the upper and lower two-dimensional (2D) layers.

In the above context, FQ-BEC phase is identified as the F-nematic phase with ferro ordering of staggered moments $\langle \mathbf{q}_i \cdot \mathbf{q}_j \rangle > 0$, breaking SU(2) down to U(1), which is previously found in the $S = \frac{1}{2}$ spin-ladder system [54]. Figure 7(d) shows the boson density $\langle n_i \rangle$ and structural factors when J'/J is varied from FQ-BEC ($J'/J < 0.15$), FQ- p -BEC ($0.15 < J'/J < 0.25$), to AFM-BEC phases. Large $\mathcal{N}(\mathbf{k})$ at the Γ point characterizes FQ-BEC, $\mathcal{C}(\mathbf{k})$ as well as $\mathcal{N}(\mathbf{k})$ at the K point take large values in FQ- p -BEC and particularly $\mathcal{C}(\mathbf{k})$ differentiates FQ- p -BEC from AFM phase.

The low-lying states of FQ- p -BEC in Fig. 7(b) have an intriguing QDJS-like structure. The states between two broken lines may form a set of ground-state manifold with $(2S + 1)$ degeneracy for each S sector, in consistency with the biaxial rotator of a 120° Néel ordering. However, these low-lying levels are not well separated from the states above them. It can be contrasted from the AFM-solid phase with 120° Néel ordering of $S = 1$ moments, exhibiting distinct $(2S + 1)$ -degenerate QDJS levels. For this, one may expect some sort of 120° long-range order of $\langle \mathbf{q}_i \rangle$ compatible with the triangular lattice geometry, which is the analog of FQ-BEC in Table I: a combined 120° order of \mathcal{S}_{i_y} in each layer, while with dimers remaining nonmagnetic. It corresponds to the NAF phase in the spin-ladder system in Ref. [54]. Instead, one can also focus only on the lowest level in each sector near the lower broken lines; their $S = 0, 3, 6$ levels at the Γ point and $S = 1, 2, 4, 5$ at the K point are symmetric under the symmetry action when putting a uniaxial rotator on triangular three sublattices, suggesting the p -nematic type of property [62]. Both \mathbf{q}_i and \mathbf{p}_i show large correlation [Fig. 7(d)], which is in agreement with the QDJS, that encloses both the 120° Néel and the p -nematic properties. One possibility is that the in-plane 120° Néel ordering of small \mathcal{S}_{i_y} exists but is not fully face to face between layers. Whereas, considering the fact that 120° Néel ordering is relatively subtle due to small moment in a standard spin- $\frac{1}{2}$ triangular lattice Heisenberg model [63], such kind of ordering may not be stable as a long-range order in our system where the activated local magnetic moment is expected to be small. The 120° $\langle \mathbf{q} \rangle$ -order may be masked by the intradimer quantum fluctuation, in which case either a pure p -nematic ordering or a more exotic spin liquid may be stabilized.

Aside from these two FQ phases, we find a conventional SN phase at $B/J \gtrsim \frac{1}{3}$ in a small region of J'/J and J''/J , which can only be detected by the Anderson tower analysis. Figure 8(a) shows the QDJS consisting of $S = 0, 2, 4, \dots$, which indicates the SU(2)-symmetry-broken SN on a triangular lattice [56]. The phase boundary between the FQ-BEC phase and SN is thus detected as the crossing of the $S = 1$

and 2 lowest excited states [see Appendix B, Fig. 12(a)]. The structure factors [Fig. 12(b)] indicate that inside the SN phase $\mathcal{Q}(\mathbf{k})$ at Γ point overwhelms $\mathcal{N}(\mathbf{k})$ at the Γ point, and vice versa for the FQ-BEC phase at $J'/J \lesssim -0.015$. The boson density in the SN phase is $\langle n_i \rangle \sim 1$ [Fig. 12(d)], consistent with the SN phase of a spin-1 BLBQ model. When B/J is large, the lowest-energy state of each dimer is a triplet, so that the bosons are fully occupied and the weak inter-dimer coupling works to exchange these triplets and generates a SN.

V. DISCUSSION

A. Origin of quadrupolar moments on a dimer bond

In the FQ-BEC and FQ- p -BEC phases of our $\mathcal{S} = 1$ effective model [Eq. (3)], the pair-creation and annihilation term \mathcal{H}_P seems to play a major role as indicated by the large energy gain e_P . To clarify the role of P , we choose the parameter $J' = -J''$ to exclude the contribution from \mathcal{J} . Then, Eq. (3) at the first-order level in J' and J'' is reduced to

$$\mathcal{H}_{\text{quad}} = -\mu \sum_{i=1}^N n_i + \sum_{\langle i,j \rangle, \alpha} [(t b_{i,\alpha}^\dagger b_{j,\alpha} + P b_{i,\alpha}^\dagger b_{j,\alpha}^\dagger) + \text{H.c.}], \quad (20)$$

which is transformed via $b_{k,\alpha}^\dagger = \frac{1}{\sqrt{N}} \sum_{i=1}^N b_{i,\alpha}^\dagger e^{-ik \cdot r_i}$ to

$$\begin{aligned} \mathcal{H}_{\text{quad}} = & \frac{1}{2} \sum_{k,\alpha} [(t\eta_k - \mu)(b_{k,\alpha}^\dagger b_{k,\alpha} + b_{k,\alpha} b_{k,\alpha}^\dagger) \\ & + P\eta_k(b_{k,\alpha}^\dagger b_{-k,\alpha}^\dagger + b_{-k,\alpha} b_{k,\alpha})] + \text{const}, \end{aligned} \quad (21)$$

where $\eta_k = 2[\cos k_x + \cos(\frac{k_x + \sqrt{3}k_y}{2}) + \cos(\frac{k_x - \sqrt{3}k_y}{2})]$. Then, using the Bogoliubov transformation

$$\begin{pmatrix} \beta_k \\ \beta_{-k}^\dagger \end{pmatrix} = \begin{pmatrix} \cosh \theta & \sinh \theta \\ \sinh \theta & \cosh \theta \end{pmatrix} \begin{pmatrix} b_k \\ b_{-k}^\dagger \end{pmatrix} \quad (22)$$

with $\tanh 2\theta = P\eta_k/(t\eta_k - \mu)$, the Hamiltonian can be diagonalized as

$$\mathcal{H}_{\text{quad}} = \sum_{k,\alpha} \varepsilon_k (\beta_{k,\alpha}^\dagger \beta_{k,\alpha} + \beta_{k,\alpha} \beta_{k,\alpha}^\dagger) + \text{const}, \quad (23)$$

where the particle-hole-symmetric energy bands are obtained as

$$\varepsilon_k = \pm \frac{1}{2} \sqrt{(t\eta_k - \mu)^2 - (P\eta_k)^2}. \quad (24)$$

Figures 9(a) and 9(b) show ε_k/J for $J' - J'' < 0$ and $J' - J'' > 0$, respectively, at $B/J = 0.2$. When the bottom of the band touches the zero level, the instability takes place and the $\beta_{k,\alpha}$ bosons of that wave number condense and form a BEC phase. This happens by increasing $J' = -J''$ only up to $|J' - J''|/J \sim 0.05$, which is consistent with the numerical analysis that the singlet product state immediately gives way to the FQ phases in the $J' = -J''$ direction. The wave number at which the ε_k takes the minimum is the Γ point when $J' - J'' < 0$, whereas it is the K point for $J' - J'' > 0$. The former is the usual uniform FQ ordering, and the latter explains well the particular three-sublattice-like structure of the quadrupole correlations in FQ- p -BEC phase we saw in Fig. 4(b).

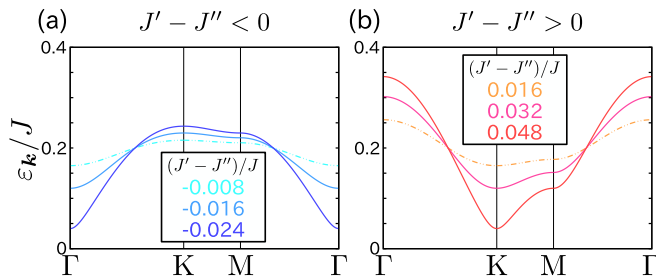


FIG. 9. Energy bands of the eigenstates of the quadratic Hamiltonian [Eq. (20)] for (a) $J' - J'' < 0$ and (b) $J' - J'' > 0$. We set $B/J = 0.2$, and use the parameters t , P , and μ defined in Eq. (4), at the first order.

B. Classification of “nematic” phases

Conventionally, a typical SN phase in spin-1 system is identified by the absence of net local-sublattice magnetic ordering and remaining quadrupolar ordering. Typically in spin-1 BLBQ models written in the form $JS_i \cdot S_j + B(S_i \cdot S_j)^2 = (J - B/2)S_i \cdot S_j + (B/2)Q_i \cdot Q_j + \text{const}$, the dipolar (magnetic) and quadrupolar orders compete with each other, and the latter appears when $|B| \gtrsim |J|$ where the magnetic ordering is suppressed. The QDJS is formed by $S = 0, 2, 4 \dots$, indicating that the $SU(2)$ symmetry is broken by the binding of two-magnon pairs.

Another series of spin nematics is a magnon-pair condensation in the spin- $\frac{1}{2}$ models [37]. Starting from the fully polarized ferromagnetic phase such as those in a high magnetic field, two-magnon instability overwhelms the one-magnon one when there is a frustration effect that prohibits the kinetic motion of a single magnon. The bound pair of magnons propagate together, which is by definition a quadrupolar order parameter itself written as $\langle b_{i\downarrow}^+ b_{j\downarrow}^+ \rangle = \langle S_i^- S_j^- \rangle = Qe^{i2\theta} \neq 0$. This bond nematics is realized when the bond is almost fully occupied by bosons; the adjacent bosons carrying $S^z = 1$ and -1 exchange or fluctuate in pairs and form a quadrupole, and accordingly the $S^z = -1$ propagate in space. It is equivalent to the spin-2 BEC in cold atoms formed by $S = 0$ and 2 sectors [64]. For a particular model that excludes the $S = 1$ sector out of the low-energy subspace, this kind of spin nematics can be found at zero field, which is characterized by the QDJS of bound bosons similar to the spin-1 BLBQ case [32,38].

These two types of ordering are categorized as n -type spin nematics, and are only possible when the $S = 1$ bosons can be bounded by a strong quantum fluctuation, mostly in a strong magnetic field that helps to increase the population of $S = 1$ bosons.

The other known class of spin nematic phase is the p -type nematic found in spin- $\frac{1}{2}$ systems [62]. The vector chirality of two spins $\mathbf{p}_i = \mathbf{S}_i \times \mathbf{S}_{i_2}$ defined on a bond [\mathbf{p}_i in Eq. (17)] condenses and forms a nematic order, again suppressing the sublattice magnetic ordering. This time the $SU(2)$ symmetry is broken down to $U(1)$ of a uniaxial rotator, and the QDJS consisting of $S = 0, 1, 2, \dots$ indicates the BEC from a one-magnon instability.

In 1D and 2D spin dimer systems, the quadrupolar moment is defined on a dimer bond. Depending on the choice of

the parameters, one can control the number of bosons from zero to one. When $\langle n_i \rangle = 1$ the same situation as the first spin-1 type of SN is realized, whereas for $\langle n_i \rangle < 1$, a BEC type of quadrupolar ordering is realized which is FQ-BEC or F-nematic. In our FQ phases, a *single* magnon condenses by the hopping and pair creation and annihilations, breaking the $SU(2)$ symmetry down to $U(1)$, which is an analog of the spinor BEC in cold atoms [65], and shares the same property as the p -type nematics. Since the dimer remains always non-magnetic, it can be regarded as some sort of “nematic” order in terms of $S = 1$ boson. When separately looking at upper- and lower-layer carrying small moments, they form a ferromagnetic sublattice long-range order, whereas the intradimer quantum fluctuation kills the moment inside the dimer, which should be regarded as a different phase from the mean-field type of interlayer AF and intralayer ferromagnetic ordering of the full spin moments observed in the ferromagnetic dimer model [41].

We saw in Sec. IV that the FQ- p -BEC phase has a strong chirality correlation and the possible 120° in-plane magnetic long-range correlation of small moments, which are masked, and the dimer unit remains nonmagnetic. There are two possibilities: in a mean-field analysis these two are incompatible, whereas our treatment treating the full quantum many-body effect may allow for a new possibility that the two types of order may coexist. The other possibility is the absence of sublattice magnetic ordering that may stabilize the p -type spin nematics. The Anderson tower does not allow for the separation of the behavior of the biaxial or uniaxial rotator, namely, the full breaking of $SU(2)$ or the breaking only down to $U(1)$ within this study.

C. Exchange of $S = 1$ moments

Previously, in a spin- $\frac{1}{2}$ dimer system [29,40], we showed that the origin of the spin nematic phase is the interdimer ring exchange interactions that permute the four spin $\frac{1}{2}$ along the twisted path as $(1, 2, 3, 4) \rightarrow (2, 3, 4, 1)$, which is shown in Fig. 10(a). In that case, the two spin $\frac{1}{2}$'s on a dimer form an $S_i = 1$ triplet, and the ring exchange interaction exchanges the spin 1's on neighboring dimers $(S_i^z, S_j^z) = (+1, -1)$ with $(-1, +1)$ states [see Fig. 10(b)], and suppress the dipolar ordering. This plays the same role as the biquadratic interaction $\mathcal{B}(S_i \cdot S_j)^2$, and when all the dimers are filled with a triplet $S_i = 1$, the system is reduced to the BLBQ model.

In the ferromagnetically coupled spin- $\frac{1}{2}$ dimer model [41], it is shown that the exchange interaction J' and J'' (J_{\parallel} and J_{\times} in their notation) operated twice at the second-order perturbation is important to stabilize the spin nematic phase. As shown schematically in Fig. 10(a), this works in the same manner as the ring exchange interaction, and generates an effective biquadratic term [66]. However, this time they need a larger J'' as their spin nematics need to compete with the stable ferromagnetic phase.

In our spin-1 dimer, the pair-creation and annihilation terms result in an off-diagonal pair condensation of up and down spin 1's via the processes shown in Fig. 10(c). These processes, when performed twice, will give the same effect as the biquadratic interaction in Fig. 10(b). The advantage here is

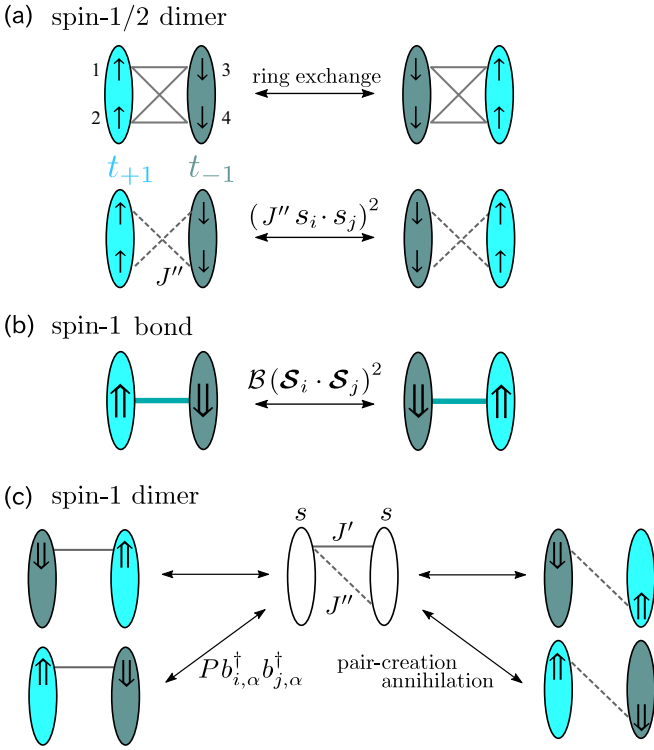


FIG. 10. Three different types of fluctuations that contribute to the formation of the spin nematics. Single and double arrows represent the spin $\frac{1}{2}$ and spin 1, respectively. (a) In the spin- $\frac{1}{2}$ dimer system, ring exchange interaction that permutes spin $\frac{1}{2}$'s as $(1, 2, 3, 4) \leftrightarrow (2, 3, 4, 1)$ in the upper panel (see Refs. [29,40]) and the second-order perturbation terms operated twice, $(J'' s_i \cdot s_j)^2$, with s_i the spin- $\frac{1}{2}$ operator discussed in Refs. [41,66], work in the similar manner. (b) Fluctuation between on-bond spin 1's that are equivalent to those of (a). (c) In our spin-1 dimer system, the pair-creation and annihilation term (P) plays a major role which originates from the first order in J' and J'' .

that it is a first-order process and can be more easily realized than B or the ring exchange processes.

The second-order perturbation process in the spin- $\frac{1}{2}$ dimer systems giving the effective biquadratic interactions can also be understood as the pair-creation and annihilation process, although in Refs. [41] and [66] it is not discussed in the spin-1 bosonic language. Nevertheless, the pair-fluctuation effect in the spin-1 dimer systems is stronger than that of spin- $\frac{1}{2}$ dimer systems; one can see from Eq. (2) that the triplet state $S = 1$ consists of twice as large dimer-spin terms than the triplets formed by two spin $\frac{1}{2}$'s, which means that the entanglement between the two $S = 1$ can be easily enhanced. We consider this to be the origin of a variety of quadrupolar phases in our system.

VI. SUMMARY AND PERSPECTIVE

In conclusion, we found various types of quadrupolar ordering in a spin-1 dimer model forming a triangular lattice bilayer. In the decoupled dimer limit, the dimer-bond hosts singlet at small B/J and triplet at larger B/J . Including the inter-dimer Heisenberg exchange terms J' and J'' , perturbatively up to second order, we derived an effective hard-core bosonic

model describing the triplet on a dimer bond, which reproduces the low-energy properties of the original model. The major part of the bosonic Hamiltonian consists of the hopping (t) and pair-creation and annihilation term (P) of bosons, as well as the chemical potential (μ) and the antiferromagnetic exchange interaction (\mathcal{J}). The bosons are doped by μ and the t term contributes to the formation of BEC. The ferromagnetic (FM) and antiferromagnetic (AFM) phases appear due to $\mathcal{J} < 0$ and $\mathcal{J} > 0$. When t and P are dominant at $J' \sim -J''$, the FQ-BEC and FQ- p -BEC phases are observed, which are the condensation of quadrupolar moments on a dimer bond, similarly to the anisotropic superfluidity in cold atoms [65]. Also, when $B/J \gtrsim \frac{1}{3}$, the typical spin-1 nematic phase is found near the interdimer decoupling ($J', J'' \sim 0$) region since each dimer is occupied by a spin-1 boson which is exchanged by P .

Our results are widely applied to the bilayer quantum spin dimer systems since the interactions appearing in Eq. (1) are all standard ones that are derived naturally from the strong-coupling perturbation theory of Mott insulator: the Heisenberg exchange interactions J , J' , and J'' and the biquadratic intradimer interaction B . The value of B is reported to be relatively larger than it has been believed before [29].

The FQ- p -BEC phases discussed here might be exotic in the sense that the distribution of $S = 1$ bosons are uniform in space, whereas the quadrupolar correlation may develop a particular spatial modulation. It differs from the SN of the $S = 1$ BLBQ model and from the multimagnon bound states of the $S = \frac{1}{2}$ models in high fields. We consider that the magnetic long-range ordering is possibly absent, and the p -nematic type of correlation develops toward the long-range ordering.

We finally discuss the relevance with the actual material. In a family of $\text{Ba}_3M\text{Ru}_2\text{O}_9$ ($M = \text{Ca}, \text{Co}, \text{Ni}, \text{Cu}, \text{Zn}, \text{Sr}$) [42–47] the two face-shared RuO_6 octahedra form a dimer which is stacked along the two-dimensional triangular lattice in the same way as our model Fig. 1(a). Since the magnetic Ru^{5+} ions and M ions are stacked along the interlayer direction as $\text{Ru-Ru-M-Ru-Ru} \dots$ with dimerized Ru 's on top of each other and M out of face, the interlayer interactions between Ru dimer layers and magnetic M layers are frustrated and weak. In fact, the antiferromagnetic ordering temperature ~ 100 K of $M = \text{Co}, \text{Ni}, \text{Cu}$ are determined by the intralayer interaction J' of the similar magnitude [46]. For nonmagnetic ions $M = \text{Ca}, \text{Zn}, \text{Sr}$, this inter-layer interaction is in principle neglected.

The magnetic moment each Ru^{5+} ion carries is expected to be $S = 1$ for several reasons; $4d^3$ electrons on t_{2g} orbitals basically form a high-spin state because of the strong Hund's coupling, and indeed the band structure calculation excludes the possibility of the “low-spin” state of $S = \frac{1}{2}$ [67]. While this may imply the $S = \frac{3}{2}$ moment from the d^3 configuration, the experiments indicate that the moments are suppressed to smaller values, e.g., 1.0–1.5 μ_B in $M = \text{Ni}$ and 1.16–1.44 μ_B in $M = \text{Cu}$ [45,46]. Since the t_{2g} orbitals are split into doubly degenerate e_g orbitals and a_{1g} orbital, the strong hybridization between a_{1g} 's of the dimerized Ru^{5+} ions is expected, generating one singlet pair of spins per dimer and reducing the spin moment of Ru^{5+} ion to $S = 1$.

Intriguing magnetic properties were reported in this family of materials: For a Zn compound, the uniform susceptibility is strongly suppressed down to 37 mK, a much lower temperature than the value of $J \sim 150\text{--}200$ K [42,43]. In a Co, Ni, or Cu compound with shorter interdimer distances, namely, having larger $|J'/J|$ and $|J''/J|$, the system undergoes an antiferromagnetic transition at $T_N \sim 100$ K [45,46]. The Ca and Sr compound with the longer interdimer distances contrarily favor a standard nonmagnetic singlet state [44]. Usually, J , J' , and J'' are antiferromagnetic ones, and if we increase the interdimer interactions from the center of the phase diagram in Fig. 2(a), where $B/J = 0.2$, toward the upper right direction, the ground state transforms from singlet, FQ- p -BEC, and to an antiferromagnetic phase, in good agreement with the experimental observation (Ca, Sr) \rightarrow (Zn) \rightarrow (Co, Ni, Cu). If the ground state of $M = \text{Zn}$ is FQ- p -BEC, one can suspect that the lack of phase transition and the suppression of magnetic ordering down to lowest temperature may fit with the ambiguous behavior of the tower of states of this phase that cannot be simply attributed to any kind of already known symmetry-breaking long-range orders.

Since the conventional SN phases were all found next to the fully polarized ferromagnetic/antiferromagnetic phase, the exotic nonmagnetic phase in the Zn compound was not really connected to the quadrupolar ordering. Our series of studies on spin dimer systems [40] point out that SN and other quadrupolar phases of spin 1 can be found next to the spin-0 singlet phase. Since this kind of symmetry breaking is not directly detected from the standard susceptibility measurements, the way to identify them experimentally should be discussed in the next step for the clarification of the unexplored nature of the spin dimer materials.

ACKNOWLEDGMENTS

We thank K. Totsuka, T. Momoi, and T. Hikihara for helpful discussions, Y. Yokoyama for advice in the early stage of this work, M. Kawano for helpful comments, and I. Terasaki for fruitful communications. This work is supported by JSPS KAKENHI Grants No. JP17K05533, No. JP18H01173, No. JP17K05497, and No. JP17H02916.

APPENDIX A: DETAILS ON THE EFFECTIVE MODEL (3)

1. Construction of a time-reversal-invariant basis of spin-1 dimer state via bond-operator approach

To make direct connections of our representation in the main text with the previous studies, we introduce the bond-operator representation of the spin-1 state in a unit of dimer. Previous bond-operator representations broke the time-reversal symmetry [50–52], which we modify to the one that keeps the time-reversal symmetry.

First, we write the time-reversal-invariant multiplet states of spin-1 dimers. Using the time-reversal-invariant basis for a single spin-1 state [18,56]

$$|x\rangle = \frac{i(|+1\rangle - |-1\rangle)}{\sqrt{2}}, \quad |y\rangle = \frac{|+1\rangle + |-1\rangle}{\sqrt{2}}, \quad |z\rangle = -i|0\rangle, \quad (\text{A1})$$

the singlet, triplet, and quintet dimer states can be rewritten as

$$|s\rangle = \frac{1}{\sqrt{3}}(|x, x\rangle + |y, y\rangle + |z, z\rangle), \quad (\text{A2})$$

$$|t_\alpha\rangle = -\frac{1}{\sqrt{2}} \sum_{\beta, \gamma} \varepsilon_{\alpha\beta\gamma} |\beta, \gamma\rangle, \quad (\text{A3})$$

$$|q_{\alpha\beta}\rangle = -\frac{1}{\sqrt{2}}(|\alpha, \beta\rangle + |\beta, \alpha\rangle) + (\sqrt{2} - 1)\delta_{\alpha\beta} |\alpha, \alpha\rangle, \quad (\text{A4})$$

respectively ($\alpha, \beta = x, y, z$). Since only three of four states $|s\rangle, |q_{\alpha\alpha}\rangle$ are linearly independent, we construct two quintet states $|q_{3\alpha^2-r^2}\rangle$ and $|q_{\beta^2-\gamma^2}\rangle$ as the linear combinations of $|q_{\alpha\alpha}\rangle$, whose forms are, for example,

$$|q_{3z^2-r^2}\rangle = \frac{2|q_{zz}\rangle - |q_{xx}\rangle - |q_{yy}\rangle}{\sqrt{6}} = -\frac{2|z, z\rangle - |x, x\rangle - |y, y\rangle}{\sqrt{6}},$$

$$|q_{x^2-y^2}\rangle = \frac{|q_{xx}\rangle - |q_{yy}\rangle}{\sqrt{2}} = -\frac{|x, x\rangle - |y, y\rangle}{\sqrt{2}}, \quad (\text{A5})$$

where we take $(\alpha, \beta, \gamma) = (z, x, y)$. We use the $|s\rangle$ and $|q_{3\alpha^2-r^2}\rangle$ and $|q_{\beta^2-\gamma^2}\rangle$ as a basis for representing $S_{i\mu}^\alpha$, namely, the choice of the basis $|q_{3\alpha^2-r^2}\rangle$ and $|q_{\beta^2-\gamma^2}\rangle$ is dependent on $\alpha = x, y, z$.

In the main text, we adopted the singlet state as a vacuum, whereas in this bond-operator approach, we redefine the vacuum as the state without any multiplet. Accordingly, instead of $b_{i,\alpha}$ and $b_{i,\alpha}^\dagger$, we use s_i (s_i^\dagger) and $t_{i,\alpha}$ ($t_{i,\alpha}^\dagger$) as the annihilation (creation) operators of the singlet and triplet of component α , and $q_{i,\alpha}$ ($q_{i,\alpha}^\dagger$) as the ones of the quintet of component α . Then, the spin-1 operator $S_{i\mu}^\alpha$ ($\mu = 1, 2$) in the i th dimer can be written as follows;

$$S_{i1}^\alpha = i\frac{\sqrt{2}}{\sqrt{3}}(t_{i,\alpha}^\dagger s_i - s_i^\dagger t_{i,\alpha}) - \frac{i}{2} \sum_{\beta, \gamma} \varepsilon_{\alpha\beta\gamma} t_{i,\beta}^\dagger t_{i,\gamma}$$

$$- \frac{i}{\sqrt{3}}(q_{i,3\alpha^2-r^2}^\dagger t_{i,\alpha} - t_{i,\alpha}^\dagger q_{i,3\alpha^2-r^2})$$

$$- \frac{i}{2} \sum_{\beta \neq \alpha} (q_{i,\alpha\beta}^\dagger t_{i,\beta} - t_{i,\beta}^\dagger q_{i,\alpha\beta}) - \frac{i}{2} \sum_{\beta, \gamma} \varepsilon_{\alpha\beta\gamma} q_{i,\alpha\beta}^\dagger q_{i,\gamma\alpha}$$

$$- \frac{i}{2} \sum_{\beta, \gamma} \varepsilon_{\alpha\beta\gamma} (q_{i,\beta^2-\gamma^2}^\dagger q_{i,\beta\gamma} - q_{i,\beta\gamma}^\dagger q_{i,\beta^2-\gamma^2}), \quad (\text{A6})$$

$$S_{i2}^\alpha = -i\frac{\sqrt{2}}{\sqrt{3}}(t_{i,\alpha}^\dagger s_i - s_i^\dagger t_{i,\alpha}) - \frac{i}{2} \sum_{\beta, \gamma} \varepsilon_{\alpha\beta\gamma} t_{i,\beta}^\dagger t_{i,\gamma}$$

$$+ \frac{i}{\sqrt{3}}(q_{i,3\alpha^2-r^2}^\dagger t_{i,\alpha} - t_{i,\alpha}^\dagger q_{i,3\alpha^2-r^2})$$

$$+ \frac{i}{2} \sum_{\beta \neq \alpha} (q_{i,\alpha\beta}^\dagger t_{i,\beta} - t_{i,\beta}^\dagger q_{i,\alpha\beta}) - \frac{i}{2} \sum_{\beta, \gamma} \varepsilon_{\alpha\beta\gamma} q_{i,\alpha\beta}^\dagger q_{i,\gamma\alpha}$$

$$- \frac{i}{2} \sum_{\beta, \gamma} \varepsilon_{\alpha\beta\gamma} (q_{i,\beta^2-\gamma^2}^\dagger q_{i,\beta\gamma} - q_{i,\beta\gamma}^\dagger q_{i,\beta^2-\gamma^2}).$$

2. Evaluation of the effective model

We examine the effect of the three-dimer interactions $\mathcal{H}_{3\text{body}}$ in the effective Hamiltonian \mathcal{H}_{eff} [Eq. (3)], which was

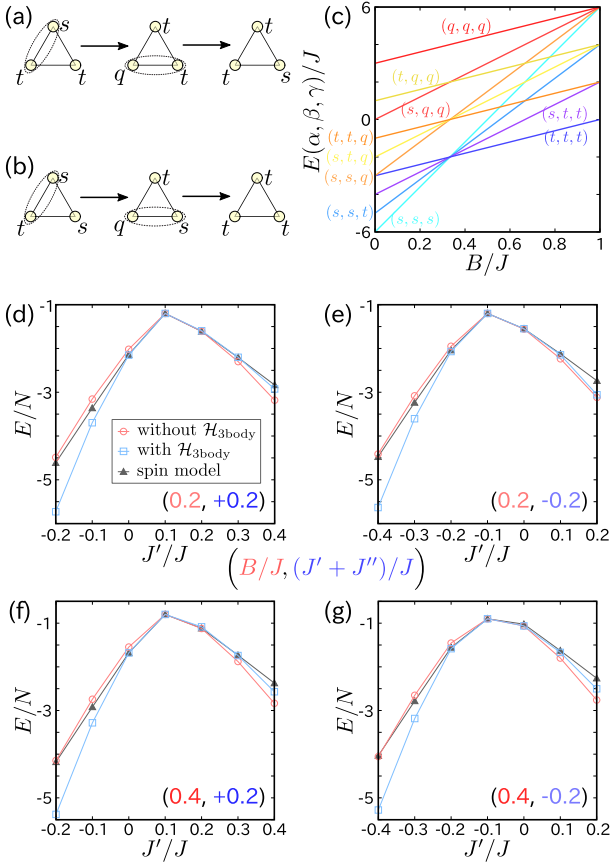


FIG. 11. (a), (b) Typical second-order perturbation processes over three-dimers. (a) Processes of “correlated hopping” and (b) pair creation of bosons. Ellipses mark the pair of sites to which the perturbation Hamiltonian $\mathcal{H}_{\text{inter}}$ operates. (c) Energy levels of $\mathcal{H}_{\text{intra}}$ of the three spin-1 dimer states. (d)–(g) J'/J dependencies of the ground-state energies of the effective Hamiltonian \mathcal{H}_{eff} with and without $\mathcal{H}_{3\text{body}}$ and the original spin Hamiltonian \mathcal{H} on the nine-dimer triangular lattice for $(B/J, (J' + J'')/J) =$ (d) $(0.2, +0.2)$, (e) $(0.2, -0.2)$, (f) $(0.4, +0.2)$, and (g) $(0.4, -0.2)$.

discarded in the calculation in the main text. First, we show some details of $\mathcal{H}_{3\text{body}}$, which originates from the three-dimer processes at the second order of perturbation. We show two examples of these processes in Figs. 11(a) and 11(b), where s , t , q are the singlet, triplet, and quintet states, respectively, on a dimer. Figure 11(a) is the process similar to the correlated hoppings found in the Shastry-Sutherland model [30,68], and Fig. 11(b) is the pair creation of bosons.

In treating these three-dimer processes, we examined the validity of restricting the low-energy manifold of states to those including only singlet and triplets. Figure 11(c) shows the energy diagram of the three-dimer states $E(\alpha, \beta, \gamma)$ ($\alpha, \beta, \gamma = s, t, q$). We see that (t, t, t) states and (s, s, q) states are degenerate at $B/J = 0$, whereas they are well separated when a small $B/J > 0$ is introduced.

Next, we compare the ground-state energies of the effective model \mathcal{H}_{eff} [Eq. (3)] with and without $\mathcal{H}_{3\text{body}}$, and the energy of the original spin-1 dimer model \mathcal{H} [Eq. (1)]. We used the nine-dimer triangular lattice under the periodic boundary condition. The cases of $B/J = 0.2$ are shown in Figs. 11(d)

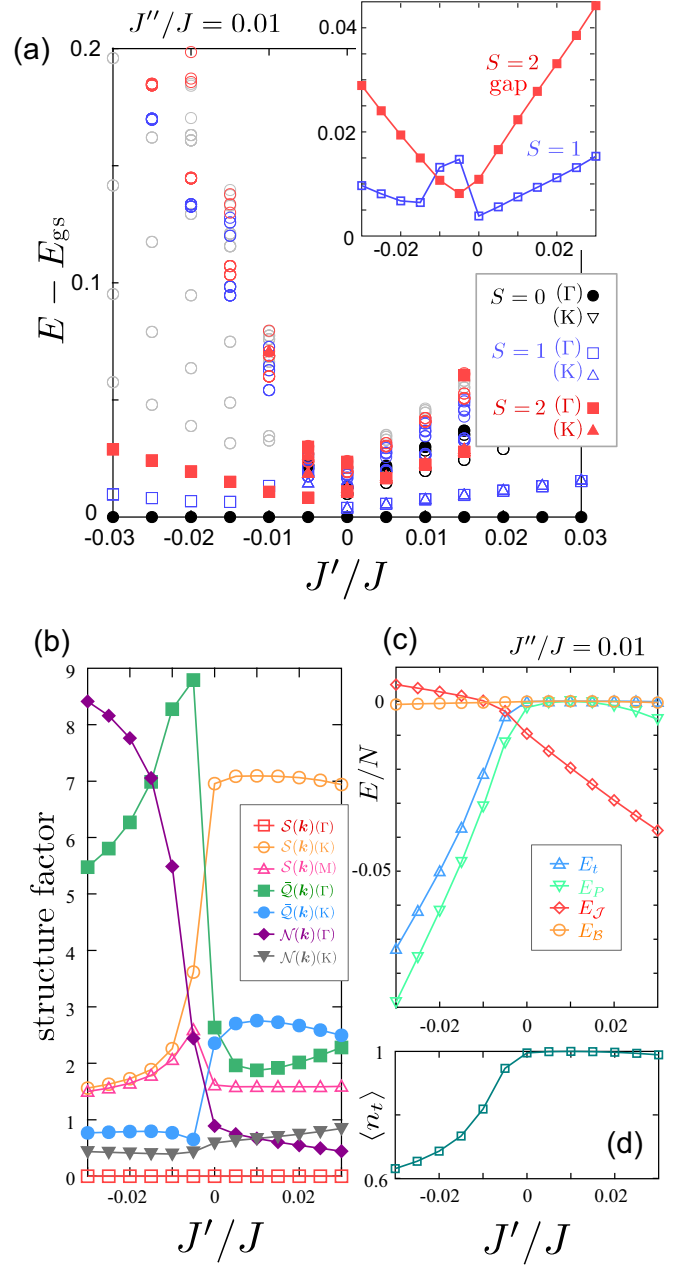


FIG. 12. (a) Low-energy excited states of $S = 0, 1, 2$ sectors as a function of small J'/J with fixed $J''/J = 0.01$, where we find a crossing of the low-lying $S = 1$ and 2 levels shown more clearly in the inset (extracted data from the main panel). The region near $J' \sim 0$ where $S = 2$ is the lowest excited state is the typical spin nematic phase found in the $S = 1$ BLBQ models. (b) Spin [Eq. (6)], quadrupole [Eq. (7)], and staggered spin [Eq. (18)] structure factors at Γ, K, M points. (c) The contributions from major terms in the effective Hamiltonian e_t, e_P, e_J , and e_B . (d) Triplet densities $\langle n_t \rangle$.

and 11(e), and those of $B/J = 0.4$ are in Figs. 11(f) and 11(g), where the parameters are chosen as $(J' + J'')/J = +0.2$ and -0.2 . It is confirmed that the energies of \mathcal{H}_{eff} with $\mathcal{H}_{3\text{dimer}}$ are not always closer to those of \mathcal{H} than those of \mathcal{H}_{eff} without $\mathcal{H}_{3\text{dimer}}$ although \mathcal{H}_{eff} with $\mathcal{H}_{3\text{dimer}}$ fully takes the second-order perturbation terms into account. We see that for $|J'/J|$ and $|J''/J| \lesssim 0.2$, the energies are in good consistency with

each other. The effective model may not hold quantitatively when either of J' , J'' has a large value. This might be because the three-dimer interactions that appear at the higher order of J' and J'' , which would cancel out the three-dimer interactions derived at the second order.

As we already saw in Sec. III B 6, the effect of second-order perturbation is small, and setting $\mathcal{H}_{3\text{body}} = 0$ does not change both the quantitative and qualitative aspects of the results. The advantage of having a simple Hamiltonian \mathcal{H}_{eff} is that it corresponds exactly to the spin- $\frac{1}{2}$ model and, resultantly, the two models of different spin numbers can be compared on equal ground.

APPENDIX B: SMALL J'/J , J''/J REGION OF THE PHASE DIAGRAM

We show the details of the physical quantities in the small J'/J , J''/J region at $B/J = 0.4$. Figure 12(a) shows the J'/J dependence of the low-energy excited states with $J''/J = 0.01$, together with the spin gaps of $\Delta S = 1$ and 2 in the inset. In varying J' , the $S = 1$ and 2 excited states cross at around $J'/J = -0.01$, which indicates the quantum phase transition from the FQ-BEC phase to the SN phase. The phase transition

is observed in the changes of the structure factors shown in Fig. 12(b), where $\mathcal{N}(\mathbf{k})$ at the Γ point is suppressed at $J'/J \sim -0.01$, and $\mathcal{Q}(\mathbf{k})$ at the Γ point solely develops.

When J' is increased further, the $S = 2$ lowest excited state again becomes higher in energy than the $S = 1$ excited state, which signals the transition from the SN phase to the AFM phase [Fig. 12(a)]. There, $\mathcal{Q}(\mathbf{k})$ becomes smaller, and $\mathcal{S}(\mathbf{k})$ at the K point develops.

Figure 12(c) shows the contributions of some terms in the effective Hamiltonian [Eq. (3)] to the ground-state energy. In the FQ-BEC phase, hoppings (e_t) and pair creation and annihilation (e_p) support the FQ-BEC phase, as discussed in Sec. V A. In the SN phase at $-0.01 \lesssim J'/J \lesssim 0$, the energy gain of e_p is still dominant. The effective biquadratic interactions generated by operating pair-creation and annihilation terms twice (see Sec. V C) play a key role, while the energy gain from the biquadratic interaction term in the Hamiltonian e_B is small. The AFM phase is stabilized by the gain e_J from the Heisenberg exchange between the $S = 1$ bosons. The J'/J dependence of the triplet density $\langle n_t \rangle$ is plotted in Fig. 12(d). In the vicinity of the phase transition from FQ-BEC to SN, the triplet density rapidly increases to $\langle n_t \rangle \sim 1$.

-
- [1] S. A. Kivelson, E. Fradkin, and V. J. Emery, *Nature (London)* **393**, 550 (1998).
- [2] M. S. Laad and L. Craco, *Phys. Rev. B* **84**, 054530 (2011).
- [3] S. Onari and H. Kontani, *Phys. Rev. Lett.* **109**, 137001 (2012).
- [4] R. M. Fernandes, A. V. Chubukov, and J. Schmalian, *Nat. Phys.* **10**, 97 (2013).
- [5] M. Blume and Y. Y. Hsieh, *J. Appl. Phys.* **40**, 1249 (1969).
- [6] A. F. Andreev and I. A. Grishchuk, *Sov. Phys. JETP* **60**, 267 (1984) [*Zh. Eksp. Teor. Fiz.* **87**, 467 (1984)].
- [7] K. Ishida, M. Morishita, K. Yawata, and H. Fukuyama, *Phys. Rev. Lett.* **79**, 3451 (1997).
- [8] T. Kimura, S. Tsuchiya, and S. Kurihara, *Phys. Rev. Lett.* **94**, 110403 (2005).
- [9] L. de Forges de Parny, H. Yang, and F. Mila, *Phys. Rev. Lett.* **113**, 200402 (2014).
- [10] L. E. Svistov, T. Fujita, H. Yamaguchi, S. Kimura, K. Omura, A. Prokofiev, A. I. Smirnov, Z. Honda, and M. Hagiwara, *JETP Lett.* **93**, 21 (2011).
- [11] Y. Kohama, H. Ishikawa, A. Matsuo, K. Kindo, N. Shannon, and Z. Hiroi, *Proc. Natl. Acad. Sci. USA* **116**, 10686 (2019).
- [12] M. Skoulatos, F. Rucker, G. J. Nilsen, A. Bertin, E. Pomjakushina, J. Ollivier, A. Schneidewind, R. Georgii, O. Zaharko, L. Keller, C. Rüegg, C. Pfleiderer, B. Schmidt, N. Shannon, A. Kriele, A. Senyshyn, and A. Smerald, *Phys. Rev. B* **100**, 014405 (2019).
- [13] H. H. Chen and P. M. Levy, *Phys. Rev. Lett.* **27**, 1383 (1971).
- [14] N. Papanicolaou, *Nucl. Phys. B* **305**, 367 (1988).
- [15] K. Tanaka, A. Tanaka, and T. Idogaki, *J. Phys. A: Math. Gen.* **34**, 8767 (2001).
- [16] K. Harada and N. Kawashima, *Phys. Rev. B* **65**, 052403 (2002).
- [17] H. Tsunetsugu and M. Arikawa, *J. Phys. Soc. Jpn.* **75**, 083701 (2006).
- [18] A. Läuchli, F. Mila, and K. Penc, *Phys. Rev. Lett.* **97**, 087205 (2006).
- [19] S. Bhattacharjee, V. B. Shenoy, and T. Senthil, *Phys. Rev. B* **74**, 092406 (2006).
- [20] A. Läuchli, G. Schmid, and S. Trebst, *Phys. Rev. B* **74**, 144426 (2006).
- [21] K. Harada, N. Kawashima, and M. Troyer, *J. Phys. Soc. Jpn.* **76**, 013703 (2007).
- [22] P. Li, G.-M. Zhang, and S.-Q. Shen, *Phys. Rev. B* **75**, 104420 (2007).
- [23] H. Tsunetsugu and M. Arikawa, *J. Phys.: Condens. Matter* **19**, 145248 (2007).
- [24] E. M. Stoudenmire, S. Trebst, and L. Balents, *Phys. Rev. B* **79**, 214436 (2009).
- [25] T. A. Tóth, A. M. Läuchli, F. Mila, and K. Penc, *Phys. Rev. B* **85**, 140403(R) (2012).
- [26] I. Niesen and P. Corboz, *Phys. Rev. B* **95**, 180404(R) (2017).
- [27] I. Niesen and P. Corboz, *SciPost Phys.* **3**, 030 (2017).
- [28] I. Niesen and P. Corboz, *Phys. Rev. B* **97**, 245146 (2018).
- [29] K. Tanaka, Y. Yokoyama, and C. Hotta, *J. Phys. Soc. Jpn.* **87**, 023702 (2018).
- [30] T. Momoi and K. Totsuka, *Phys. Rev. B* **62**, 15067 (2000).
- [31] T. Momoi and N. Shannon, *Prog. Theor. Phys. Suppl.* **159**, 72 (2005).
- [32] N. Shannon, T. Momoi, and P. Sindzingre, *Phys. Rev. Lett.* **96**, 027213 (2006).
- [33] T. Momoi, P. Sindzingre, and N. Shannon, *Phys. Rev. Lett.* **97**, 257204 (2006).
- [34] T. Hikihara and S. Yamamoto, *J. Phys. Soc. Jpn.* **77**, 014709 (2008).
- [35] T. Hikihara, L. Kecke, T. Momoi, and A. Furusaki, *Phys. Rev. B* **78**, 144404 (2008).

- [36] J. Sudan, A. Lüscher, and A. M. Läuchli, *Phys. Rev. B* **80**, 140402(R) (2009).
- [37] M. E. Zhitomirsky and H. Tsunetsugu, *Europhys. Lett.* **92**, 37001 (2010).
- [38] T. Momoi, P. Sindzingre, and K. Kubo, *Phys. Rev. Lett.* **108**, 057206 (2012).
- [39] Z. Wang and C. D. Batista, *Phys. Rev. Lett.* **120**, 247201 (2018).
- [40] Y. Yokoyama and C. Hotta, *Phys. Rev. B* **97**, 180404(R) (2018).
- [41] T. Hikihara, T. Misawa, and T. Momoi, *Phys. Rev. B* **100**, 214414 (2019).
- [42] I. Terasaki, T. Igarashi, T. Nagai, K. Tanabe, H. Taniguchi, T. Matsushita, N. Wada, A. Takata, T. Kida, M. Hagiwara, K. Kobayashi, H. Sagayama, R. Kumai, H. Nakao, and Y. Murakami, *J. Phys. Soc. Jpn.* **86**, 033702 (2017).
- [43] T. D. Yamamoto, H. Taniguchi, and I. Terasaki, *J. Phys.: Condens. Matter* **30**, 355801 (2018).
- [44] J. Darriet, M. Drillon, G. Villeneuve, and P. Hagenmuller, *J. Solid State Chem.* **19**, 213 (1976).
- [45] P. Lightfoot and P. D. Battle, *J. Solid State Chem.* **89**, 174 (1990).
- [46] J. T. Rijssenbeek, Q. Huang, R. W. Erwin, H. W. Zandbergen, and R. J. Cava, *J. Solid State Chem.* **146**, 65 (1999).
- [47] P. Beran, S. A. Ivanov, P. Nordblad, S. Middey, A. Nag, D. D. Sarma, S. Ray, and R. Mathieu, *Solid State Sci.* **50**, 58 (2015).
- [48] A. V. Chubukov, *JETP Lett.* **49**, 129 (1989) [*Pis'ma Zh. Eksp. Teor. Fiz.* **49**, 108 (1989)].
- [49] S. Sachdev and R. N. Bhatt, *Phys. Rev. B* **41**, 9323 (1990).
- [50] W. Brenig and K. W. Becker, *Phys. Rev. B* **64**, 214413 (2001).
- [51] H.-T. Wang, H. Q. Lin, and J.-L. Shen, *Phys. Rev. B* **61**, 4019 (2000).
- [52] B. Kumar, *Phys. Rev. B* **82**, 054404 (2010).
- [53] P. Lecheminant and K. Totsuka, *Phys. Rev. B* **74**, 224426 (2006).
- [54] K. Totsuka, P. Lecheminant, and S. Capponi, *Phys. Rev. B* **86**, 014435 (2012).
- [55] T. Nikuni, M. Oshikawa, A. Oosawa, and H. Tanaka, *Phys. Rev. Lett.* **84**, 5868 (2000).
- [56] K. Penc and A. M. Läuchli, Spin Nematic Phases in Quantum Spin Systems, in *Introduction to Frustrated Magnetism*, edited by C. Lacroix, P. Mendels, and F. Mila (Springer, Berlin, 2011), Chap. 13, p. 331.
- [57] A. Wietek, M. Schuler, and A. M. Läuchli [arXiv:1704.08622](https://arxiv.org/abs/1704.08622).
- [58] K. Wu and H. Simon, *SIAM J. Matrix Anal. Appl.* **22**, 602 (2000).
- [59] P. W. Anderson, *Phys. Rev.* **86**, 694 (1952).
- [60] B. Bernu, C. Lhuillier, and L. Pierre, *Phys. Rev. Lett.* **69**, 2590 (1992).
- [61] B. Bernu, P. Lecheminant, C. Lhuillier, and L. Pierre, *Phys. Rev. B* **50**, 10048 (1994).
- [62] A. Läuchli, J. C. Domenge, C. Lhuillier, P. Sindzingre, and M. Troyer, *Phys. Rev. Lett.* **95**, 137206 (2005).
- [63] F. Mezzacapo and J. I. Cirac, *New J. Phys.* **12**, 103039 (2010).
- [64] M. Ueda and M. Koashi, *Phys. Rev. A* **65**, 063602 (2002).
- [65] T.-L. Ho, *Phys. Rev. Lett.* **81**, 742 (1998).
- [66] T. Hikihara and O. A. Starykh, *Phys. Rev. B* **81**, 064432 (2010).
- [67] S. V. Streltsov, *Phys. Rev. B* **88**, 024429 (2013).
- [68] T. Momoi and K. Totsuka, *Phys. Rev. B* **61**, 3231 (2000).